# Optimal Design of Natural and Hybrid Laminar Flow Control on Wings

by

Jan Pralits

October 2003
Technical Reports from
Royal Institute of Technology
Department of Mechanics
SE-100 44 Stockholm, Sweden

Typsatt i $\mathcal{AMS}$-LaTeX.

Akademisk avhandling som med tillstånd av Kungliga Tekniska Högskolan i Stockholm framlägges till offentlig granskning för avläggande av teknologie doktorsexamen onsdagen den 7:e oktober 2003 kl. 10.15 i Kollegiesalen, Administrationsbyggnaden, Kungliga Tekniska Högskolan, Valhallavägen 79, Stockholm.



Universitetsservice, Stockholm 2003

**Optimal design of natural and hybrid laminar flow control on wings.**

Jan Pralits
Department of Mechanics, Royal Institute of Technology
SE-100 44 Stockholm, Sweden.

## Abstract

Methods for optimal design of different means of control are developed in this thesis. The main purpose is to maintain the laminar flow on wings at a chord Reynolds number beyond what is usually transitional or turbulent. Linear stability analysis is used to compute the exponential amplification of infinitesimal disturbances, which can be used to predict the location of laminar-turbulent transition. The controls are computed using gradient-based optimization techniques where the aim is to minimize an objective function based upon, or related to, the disturbance growth. The gradients of the objective functions with respect to the controls are evaluated from the solutions of adjoint equations.

Sensitivity analysis using the gradients of the disturbance kinetic energy with respect to different periodic forcing show where and by what means control is most efficiently made. The results are presented for flat plate boundary layer flows with different free stream Mach numbers.

A method to compute optimal steady suction distributions to minimize the disturbance kinetic energy is presented for both incompressible and compressible boundary layer flows. It is shown how to formulate an objective function in order to minimize simultaneously different types of disturbances which might exist in two, and three-dimensional boundary layer flows. The problem formulation also includes control by means of realistic pressure chambers, and results are presented where the method is applied on a swept wing designed for commercial aircraft.

Optimal temperature distributions for disturbance control are presented for flat plate boundary layer flows. It is shown that the efficiency of the control depends both on the free stream Mach number, and whether the wall downstream of the control domain is insulated, or heat transfer occurs.

Shape optimization is presented with the aim of reducing the aerodynamic drag, while maintaining operational properties. Results of optimized airfoils are presented for cases where both the disturbance kinetic energy, and wave drag are reduced simultaneously while lift, and pitch-moment coefficients as well as the volume are kept at desired values.

**Descriptors:** fluid mechanics, laminar-turbulent transition, boundary layer, laminar flow control, natural laminar flow, adjoint equations, optimal control, objective function, PSE, APSE, ABLE, HLFC, $e^N$-method, Euler equations

# Preface

The thesis is based on and contains the following papers:

**Paper 1.** Pralits, J. O., Airiau, C., Hanifi, A. & Henningson, D. S. 2000 Sensitivity analysis using adjoint parabolized stability equations for compressible flows. *Flow, Turbulence and Combustion*, **65**(3), 312–346

**Paper 2.** Pralits, J. O., Hanifi, A. & Henningson, D. S. 2002 Adjoint-based optimization of steady suction for disturbance control in incompressible flows. *Journal of Fluid Mechanics*, **467**, 129–161

**Paper 3.** Pralits, J. O. & Hanifi, A. 2003 Optimization of steady suction for disturbance control on infinite swept wings. *Physics of Fluids*, **15**(9), 2756–2772

**Paper 4.** Pralits, J. O. & Hanifi, A. 2003 Optimization of steady wall temperature for disturbance Control. To be submitted.

**Paper 5.** Amoignon, O., Pralits, J. O., Hanifi, A., Berggren, M. & Henningson, D. S. 2003 Shape optimization for delay of laminar-turbulent transition. *Technical Report FOI-R–0919–SE, at the Swedish Defence Research Agency, FOI, Aeronautics Division, FFA.*

The papers are re-set in the present thesis format.

**Reports and proceedings related to the content of the thesis**

Pralits, J. O., Hanifi, A. & Henningson, D. S. 2000 Adjoint-based Suction Optimization for 3D Boundary Layer Flows. *Technical Report FFA TN 2000-58, at the Swedish Defence Research Agency, FOI, Aeronautics Division, FFA.*

Airiau C., Pralits, J. O., Bottaro, A. & Hanifi, A. 2001 Adjoint PSE and boundary layer equations for HLFC. *Technical Report TR 10, ALTTA Deliverable No D3.1.4-1.*

Hanifi, A., Pralits, J. O., Zuccher, S, Donelli, R. & Airiau, C. 2001 Adjoint-based Sensitivity Analysis: Validation and Comparison. *Technical Report TR 22, ALTTA Deliverable No D3.1.4-2.*

Pralits, J. O., Hanifi, A. & Mughal, S. 2002 Optimal suction design for HLFC applications. *Technical Report TR 57, ALTTA Deliverable No D3.1.4-6.*

Pralits, J. O.& Hanifi, A. 2002 Optimization of Steady Suction for Disturbance Control on Infinite Swept Wings. *In proceeding no. FEDSM2002-31055 at ASME Fluids Engineering Division Summer Meeting, Montreal, Canada.*

Pralits, J. O.& Hanifi, A. 2003 Optimal Suction Design for HLFC Applications. *AIAA paper 2003-4164, 33rd AIAA Fluid Dynamics Conference and Exhibit, Orlando, Florida.*

# Contents

# Part 1

# Summary

CHAPTER 1

# Introduction

The final design of an aircraft wing is always a compromise in the intersection of feasibility imposed by various requirements. Aerodynamics is one important aspect as it enables calculations of operational properties such as lift, moments and drag. Traditionally, the design work has been an iterative process between theory and experiments, in which the latter has often been costly. Orville and Wilbur Wright[1] spend many hours in the laboratory using their home made wind tunnel to test different types of wings in order to increase the lift coefficient enough enabling their first controlled flight in 1903. Nowadays, when available computer power increases rapidly and numerical tools increase in accuracy and modeling capability, both experiments and numerical calculations are part of the total design process. For a computational method to be reliable as a tool, it must be based on a mathematical model which provides an appropriate representation of the significant features of the flow, such as shock waves, boundary layers and laminar-turbulent transition.

The total drag of an aircraft is mainly given by the sum of pressure or wave drag, related to the existence of shock waves for transonic and supersonic flows, and viscous drag, whose magnitude depends on whether the flow is laminar or turbulent. Turbulent flow, in some cases, produces a much larger drag; thus important research efforts have been devoted to find efficient means to keep the flow laminar over the largest possible portion of the wing surface. A similar situation is encountered in other industrial applications (wind-turbine blades, diffuser inlets), where less turbulence means less energy spent to achieve the same motion, which in turn translates directly to less pollution and reduced expenses.

Control of fluid flow can be made by means of *active* or *passive* control devices. A natural passive device is the shape of the wing itself, and reduction of drag is obtained by a properly made design. An approach in which the aim is to increase the laminar portion of the wing is usually called Natural Laminar Flow (NLF) design. Other examples are found looking at the surface structure where roughness elements or cavities, such as on golf-balls, are sometimes used. An active device which has been investigated extensively is suction of air through the whole or parts of the wing which have been equipped with a porous surface. This technique falls into the category of Laminar Flow Control (LFC) which

[1] The 17th of December 2003 is the 100 year anniversary of the first controlled flight performed by O. and W. Wright in 1903 which had a duration of 59 seconds.

means to maintain the laminar flow at a chord Reynolds number beyond what is usually transitional or turbulent when no control is used. With this definition it does not cover cases where the aim is to relaminarize already turbulent flow. A combination of NLF and LFC in which the active control is imposed only on a part of the wing is usually called Hybrid Laminar Flow Control (HLFC). A distinctive feature of any flow design process as opposed to one not involving fluids is that the computation is often very costly, or even totally out of reach of any existing computer when turbulent flow in complex geometries is involved. It is therefore common practice to introduce approximations. Once a reliable and efficient numerical tool is available, a straight-forward approach for design of passive or active devices is a vast parameter study in order to find the control which best meets certain criteria set on the operational properties, and decreases the drag. In most cases the number of possible designs is large, and it is very unlikely that a truly optimal design can be found without assistance of automatic tools. For this reason, there is a growing interest in utilizing numerical optimization techniques to assist in the aerodynamic design process.

The aim of the work presented in this thesis is to integrate physical modeling of the flow and modern optimization techniques in order to perform optimal NLF and HLFC design. Gradient-based optimization techniques are used and the gradients of interest are derived using adjoint equations. When one considers highly streamlined bodies such as wings, there is often a substantial laminar portion, thus a correct transition prediction becomes essential for a good estimate of the total drag. The governing equations for the physical problem are introduced in chapter 2, and transition prediction is covered in chapter 3. Means of control laminar-turbulent transition is discussed in 4, and the approach taken here to perform optimal HLFC and NLF is given in chapter 5. A summary and conclusions are given in chapter 6, and papers related to the work presented in these chapters are given in the second part.

CHAPTER 2

# Modeling the flow

## 2.1. Governing equations

The motion of a compressible gas is given by the conservation equations of mass, momentum and energy and the equation of state. The conservation equations in dimensionless form and vector notation are

$$\frac{\partial \rho}{\partial t} + \nabla \cdot (\rho \mathbf{u}) = 0, \tag{2.1}$$

$$\rho\Big[\frac{\partial \mathbf{u}}{\partial t} + (\mathbf{u}\cdot\nabla)\mathbf{u}\Big] = -\nabla p + \frac{1}{Re}\nabla\Big[\lambda(\nabla\cdot\mathbf{u})\Big] + \frac{1}{Re}\nabla\cdot\Big[\mu(\nabla\mathbf{u} + \nabla\mathbf{u}^{\mathrm{T}})\Big], \tag{2.2}$$

$$\rho c_p\Big[\frac{\partial T}{\partial t} + (\mathbf{u}\cdot\nabla)T\Big] = \frac{1}{Re\,\mathrm{Pr}}\nabla\cdot(\kappa\nabla T) + (\gamma-1)M^2\Big[\frac{\partial p}{\partial t} + (\mathbf{u}\cdot\nabla)p + \frac{1}{Re}\Phi\Big], \tag{2.3}$$

$$\gamma M^2 p = \rho T, \tag{2.4}$$

with viscous dissipation given as

$$\Phi = \lambda(\nabla\cdot\mathbf{u})^2 + \frac{1}{2}\mu\Big[\nabla\mathbf{u} + \nabla\mathbf{u}^{\mathrm{T}}\Big]^2.$$

Here $t$ represents time, $\rho, p, T$ stand for density, pressure and temperature, $\mathbf{u}$ is the velocity vector. The quantities $\lambda, \mu$ stand for the second and dynamic viscosity coefficients, $\gamma$ is the ratio of specific heats, $\kappa$ the heat conductivity and $c_p$ the specific heat at constant pressure. All flow quantities are made dimensionless by corresponding reference flow quantities at a fixed streamwise position $x_0^\star$, except the pressure which is made dimensionless with two times the corresponding dynamic pressure. The reference length scale is fixed and taken as

$$l_0^\star = \sqrt{\frac{\nu_0^\star x_0^\star}{U_0^\star}}.$$

The Mach number, $M$, Prandtl number, Pr and Reynolds number, $Re$ are defined as

$$M = \frac{U_0^\star}{\sqrt{\Re\gamma T_0^\star}}, \quad \mathrm{Pr} = \frac{\mu_0^\star c_{p0}^\star}{\kappa_0^\star}, \quad Re = \frac{U_0^\star l_0^\star}{\nu_0^\star},$$

where $\Re$ is the specific heat constant and superscript $^\star$ refers to dimensional quantities. In order to generalize the equations for geometries with curved surfaces an orthogonal curvilinear coordinate system is introduced. The transformation from Cartesian coordinates $X^i$ to curvilinear coordinates $x^i$ is made

using the scale factors $h_i$. The definition of the scale factors and corresponding derivatives $m_{ij}$ are given as

$$h_i^2 = \sum_{j=1}^{3} \Big( \frac{\partial X^j}{\partial x^i} \Big)^2 \qquad \text{and} \qquad m_{ij} = \frac{1}{h_i h_j} \frac{\partial h_i}{\partial x^j}.$$

Using the scale factors, an arc length in this coordinate system can be written as

$$ds^2 = \sum_{i=1}^{3} \Big( h_i dx^i \Big)^2.$$

Here, $x^1$, $x^2$ and $x^3$ are the coordinates of the streamwise, spanwise and wall normal directions respectively[1].

## 2.2. The steady boundary layer flow

In this thesis flat plate boundary-layer flows with and without pressure gradient are considered as well as the flow past a swept wing with infinite span. All these different flows are special cases of the flow past a swept wing with infinite span. They are here given in dimensionless primitive variable form as

$$\frac{1}{h_1}\frac{\partial(\rho U)}{\partial x^1} + \frac{\partial(\rho W)}{\partial x^3} = 0, \tag{2.5}$$

$$\frac{\rho U}{h_1}\frac{\partial U}{\partial x^1} + \rho W \frac{\partial U}{\partial x^3} = -\frac{1}{h_1}\frac{dP_e}{dx^1} + \frac{1}{Re}\frac{\partial}{\partial x^3}\Big(\mu \frac{\partial U}{\partial x^3}\Big), \tag{2.6}$$

$$\frac{\rho U}{h_1}\frac{\partial V}{\partial x^1} + \rho W \frac{\partial V}{\partial x^3} = \frac{1}{Re}\frac{\partial}{\partial x^3}\Big(\mu \frac{\partial V}{\partial x^3}\Big), \tag{2.7}$$

$$\begin{aligned} c_p \frac{\rho U}{h_1}\frac{\partial T}{\partial x^1} + c_p \rho W \frac{\partial T}{\partial x^3} &= \frac{1}{RePr}\frac{\partial}{\partial x^3}\Big(\kappa \frac{\partial T}{\partial x^3}\Big) \\ &+ (\gamma - 1)M^2 \Big\{ \frac{U}{h_1}\frac{dP_e}{dx^1} + \frac{\mu}{Re}\Big[ \Big(\frac{\partial U}{\partial x^3}\Big)^2 + \Big(\frac{\partial V}{\partial x^3}\Big)^2 \Big] \Big\}, \end{aligned} \tag{2.8}$$

where $U, V, W$ are the streamwise, spanwise and wall-normal velocity components, respectively[2]. Under the boundary-layer assumptions, the pressure is constant in the direction normal to the wall, i. e. $P = P_e(x^1)$. The equation of state can then be expressed as

$$\gamma M^2 P_e = \rho T,$$

and the streamwise derivative of the pressure is given by the inviscid flow as

$$\frac{dP_e}{dx^1} = -\rho_e U_e \frac{dU_e}{dx^1}.$$

[1] In the second paper the coordinates are given as $x^1 = x$, $x^2 = z$ and $x^3 = y$, where $x, y, z$ are the streamwise, wall normal and spanwise coordinates, respectively.

[2] In the second paper $U, V, W$ are the streamwise, wall normal and spanwise velocity components respectively.

The corresponding boundary conditions with no-slip conditions and assuming an adiabatic wall condition are

$$U = V = W = \frac{\partial T}{\partial x^3} = 0, \qquad \text{at} \qquad x^3 = 0,$$
$$(U, V, T) \to (U_e, V_e, T_e), \qquad \text{as} \qquad x^3 \to +\infty.$$

The variables with subscript $e$ are evaluated at the boundary layer edge and are calculated from well known fundamental relations using respective free stream values found either from measurements or inviscid flow calculations. The first relation is that the total enthalpy is constant along a streamline in an inviscid, steady, and adiabatic flow. The second is the isentropic relations which are used to obtain the relation between pressure, density and temperature expressed as ratios between total and static quantities.

## 2.3. Linear stability equations

In order to derive the linear stability equations, we decompose the total flow field $q$ and material quantities into a mean $\bar{q}$, and a perturbation part $\tilde{q}$ as

$$q(x^1, x^2, x^3, t) = \bar{q}(x^1, x^2, x^3) + \tilde{q}(x^1, x^2, x^3, t) \tag{2.9}$$

where $\bar{q} \in [U, V, W, p, T, \rho]$ and $\tilde{q} \in [\tilde{u}, \tilde{v}, \tilde{w}, \tilde{p}, \tilde{T}, \tilde{\rho}]$. The mean flow quantities were introduced in the previous sections and the lower case variables correspond the the disturbance quantities. It is assumed that $c_p, \mu$ and $\kappa$ are functions of the temperature only and are divided into a mean and perturbation part. The latter are expressed as expansions in temperature as

$$\tilde{c}_p = \frac{dc_p}{dT}\tilde{T}, \qquad \tilde{\mu} = \frac{d\mu}{dT}\tilde{T}, \qquad \tilde{\kappa} = \frac{d\kappa}{dT}\tilde{T}.$$

The ratio of the coefficients of second and dynamic viscosity is given as

$$\frac{\lambda}{\mu} = \frac{\mu_v}{\mu} - \frac{2}{3}, \tag{2.10}$$

were the bulk viscosity $\mu_v$ is given as

$$\frac{\mu_v(T)}{\mu(T)} = \Big(\frac{\mu_v}{\mu}\Big)_{T=293.3\ K} \exp\Big(\frac{T - 293.3}{1940}\Big),$$

and is taken from Bertolotti (1998). Note here that Stokes' hypothesis is used setting $\mu_v = 0$ in expression (2.10). We introduce the flow decomposition (2.9) into the governing equations (2.1)–(2.4), subtract the mean flow, and neglect non-linear disturbance terms. The result can be written as

$$\frac{\mathrm{D}\tilde{\rho}}{\mathrm{D}t} + \rho\nabla\cdot\tilde{\mathbf{u}} + \tilde{\rho}\nabla\cdot\mathbf{u} + \tilde{\mathbf{u}}\cdot\nabla\rho = 0, \tag{2.11}$$

$$\rho\Big[\frac{\mathrm{D}\tilde{\mathbf{u}}}{\mathrm{D}t} + (\tilde{\mathbf{u}}\cdot\nabla)\mathbf{u}\Big] + \tilde{\rho}(\mathbf{u}\cdot\nabla)\mathbf{u} = -\nabla\tilde{p} + \frac{1}{Re}\nabla\Big[\lambda(\nabla\cdot\tilde{\mathbf{u}}) + \tilde{\lambda}(\nabla\cdot\mathbf{u})\Big] + \frac{1}{Re}\nabla\cdot\Big[\mu(\nabla\tilde{\mathbf{u}} + \nabla\tilde{\mathbf{u}}^{\mathrm{T}}) + \tilde{\mu}(\nabla\mathbf{u} + \nabla\mathbf{u}^{\mathrm{T}})\Big], \tag{2.12}$$

$$\rho c_p\Big[\frac{\mathrm{D}\tilde{T}}{\mathrm{D}t}+(\tilde{\mathbf{u}}\cdot\nabla)T\Big]+(\rho\tilde{c_p}+\tilde{\rho}c_p)(\mathbf{u}\cdot\nabla)T=\frac{1}{Re\,\mathrm{Pr}}\nabla\cdot(\kappa\nabla\tilde{T})$$
$$+\frac{1}{Re\,\mathrm{Pr}}\nabla\cdot(\tilde{\kappa}\nabla T)+(\gamma-1)M^2\Big[\frac{\mathrm{D}\tilde{p}}{\mathrm{D}t}+(\tilde{\mathbf{u}}\cdot\nabla)p+\frac{1}{Re}\tilde{\Phi}\Big],\quad(2.13)$$
$$\gamma M^2\tilde{p}=\rho\tilde{T}+\tilde{\rho}T,\quad(2.14)$$

where

$$\frac{\mathrm{D}}{\mathrm{D}t}=\frac{\partial}{\partial t}+\mathbf{u}\cdot\nabla$$

and

$$\tilde{\Phi}=\tilde{\lambda}(\nabla\cdot\mathbf{u})^2+2\lambda\Big[(\nabla\cdot\mathbf{u})(\nabla\cdot\tilde{\mathbf{u}})\Big]+\mu(\nabla\mathbf{u}+\nabla\mathbf{u}^{\mathrm{T}}):(\nabla\tilde{\mathbf{u}}+\nabla\tilde{\mathbf{u}}^{\mathrm{T}})$$
$$+\frac{1}{2}\tilde{\mu}(\nabla\mathbf{u}+\nabla\mathbf{u}^{\mathrm{T}}):(\nabla\mathbf{u}+\nabla\mathbf{u}^{\mathrm{T}}),\quad(2.15)$$

with the definition $A:B=A_{ij}B_{ij}$. These equations are subject to the following boundary conditions:

$$\tilde{u}=\tilde{v}=\tilde{w}=\tilde{T}=0,\qquad\text{at}\qquad x^3=0,$$
$$(\tilde{u},\tilde{v},\tilde{w},\tilde{T})\to 0,\qquad\text{as}\qquad x^3\to+\infty.$$

## 2.4. Parabolized stability equations

In most cases a boundary layer grows in the downstream direction. In classical or quasi-parallel stability theory the parallel-flow assumption is made which means that the growth of the boundary layer is not taken into account. Setting the non-parallel terms to zero is commonly made on grounds that the growth of the boundary layer is small over a wave length of the disturbances and that the local boundary layer profiles will determine the behavior of the disturbances. This is an additional approximation made on the linearized equations which for instance has to be considered in comparisons between theory and experiments. Theoretical investigations of the instability of growing boundary layers can be found in e. g. Gaster (1974); Saric & Nayfeh (1975) who used a method of successive approximations and a multiple-scales method, respectively. In Hall (1983), the idea of solving the parabolic disturbance equations was introduced to investigate the linear development of Görtler vortices. Parabolic equations for the development of small-amplitude Tollmien-Schlichting waves was developed by Itoh (1986). Further development was done by e. g. Herbert & Bertolotti (1987); Bertolotti *et al.* (1992) who derived the non-linear Parabolized Stability Equations (PSE). Simen (1992) developed independently a similar theory for the development of convectively amplified waves propagating in non-uniform flows. The PSE has since its development been used to investigate different kind of problems such as stability analysis of different types of flows (Bertolotti *et al.* 1992; Malik & Balakumar 1992), receptivity studies (Hill 1997a; Airiau 2000; Dobrinsky & Collis 2000), sensitivity analysis (Pralits *et al.* 2000) and optimal control problems (Hill 1997b; Pralits *et al.* 2002; Walther *et al.* 2001; Pralits & Hanifi 2003; Airiau *et al.* 2003). In the

following sections an outline based on Hanifi *et al.* (1994) is given on the derivation of the parabolized stability equations used in this thesis. A review of the PSE can be found in Herbert (1997).

### 2.4.1. *Assumption and derivation*

The disturbance equations are derived for mean flows which are independent of the $x^2$ direction i. e. quasi-three dimensional flows. Two assumptions are used in the derivation:

**1.** The first is of WKB (Wentzel, Kramers and Brillouin) type in which the dependent variables are divided into a amplitude and a oscillating part as

$$\tilde{\mathbf{q}}(x^i, t) = \hat{\mathbf{q}}(x^1, x^3) e^{i\theta} \tag{2.16}$$

where $\tilde{\mathbf{q}}$ is the complex amplitude function and $i$ the imaginary unit,

$$\theta = \int_{X_0}^{x^1} \alpha(x')\, dx' + \beta x^2 - \omega t$$

the complex wave function with angular frequency $\omega$, streamwise and spanwise wave numbers $\alpha$ and $\beta$, respectively. Note that both the amplitude and wave functions depend on the $x^1$-direction.

**2.** The second assumption is a scale separation $Re_0^{-1}$ between the weak variation in the $x^1$-direction and the strong variation in the $x^3$-direction. Here, $Re_0$ is the local Reynolds number at a streamwise position $x_0$. Further, the wall normal component of the mean flow $W$ and the derivatives of the scale factors $m_{ij}$ are also assumed to scale with $Re_0^{-1}$. A slow scale $x_S^1 = x^1 Re_0^{-1}$ is introduced which gives the new dependent variables

$$\begin{aligned} h_i &= h_i(x_S^1, x^3 Re_0^{-1}), \\ \bar{\mathbf{q}} = \bar{\mathbf{q}}(x_S^1, x^3), &\qquad W = W_S(x_S^1, x^3) Re_0^{-1}, \\ \hat{\mathbf{q}} = \hat{\mathbf{q}}(x_S^1, x^3), &\qquad \alpha = \alpha(x_S^1). \end{aligned} \tag{2.17}$$

If the ansatz (2.16) and the scalings (2.17) are introduced in the linearized governing equations, keeping terms up to $(Re_0^{-1})$, we obtain the linear parabolized stability equations. They can be written in the form

$$\mathcal{A}\hat{\mathbf{q}} \;+\; \mathcal{B}\frac{1}{h_3}\frac{\partial \hat{\mathbf{q}}}{\partial x^3} \;+\; \mathcal{C}\frac{1}{h_3^2}\frac{\partial^2 \hat{\mathbf{q}}}{(\partial x^3)^2} \;+\; \mathcal{D}\frac{1}{h_1}\frac{\partial \hat{\mathbf{q}}}{\partial x^1} \;=\; 0, \tag{2.18}$$

where $\hat{\mathbf{q}} = (\hat{\rho}, \hat{u}, \hat{v}, \hat{w}, \hat{T})^{\mathrm{T}}$. These equations describe the non-uniform propagation and amplification of wave-type disturbances in a non-uniform mean flow. The non-zero coefficients of the $5 \times 5$ matrices $\mathcal{A}, \mathcal{B}, \mathcal{C}$ and $\mathcal{D}$ are found in Pralits *et al.* (2000). Equation (2.18) is a set of nearly parabolic partial differential equations (see section 2.4.2). The boundary conditions of the disturbances at the wall and in the freestream are

$$\begin{aligned} \hat{u} = \hat{v} = \hat{w} = \hat{T} = 0, &\qquad \text{at} \qquad x^3 = 0, \\ (\hat{u}, \hat{v}, \hat{w}, \hat{T}) \to 0, &\qquad \text{as} \qquad x^3 \to +\infty. \end{aligned}$$

Note that in the ansatz (2.16), both the amplitude and wave functions given above depend on the $x^1$-direction. To remove this ambiguity, a *normalization* or *auxiliary* condition is introduced such that the streamwise variation of the amplitude function remains small. This is in accordance with the WKB type assumption where the amplitude function should vary slowly on the scale of a wavelength. Various forms of the normalization condition exist (see Hanifi *et al.* 1994). In the investigations presented here we have used the following condition

$$\int_0^{+\infty} \hat{\mathbf{q}}^{\mathrm{H}} \frac{\partial \hat{\mathbf{q}}}{\partial x^1}\, dx^3 = 0, \tag{2.19}$$

where superscript H denotes the conjugate transpose. The stability equation (2.18) is integrated in the downstream direction initiated at an upstream position $x^1 = X_0$ with the initial condition $\tilde{q} = \tilde{q}_0$ given by the local stability theory. At each streamwise position the streamwise wavenumber $\alpha$ is iterated such that the normalization condition (2.19) is satisfied. When a converged streamwise wave number has been obtained the disturbance growth rate $\sigma$ can be calculated. For an arbitrary disturbance component $\xi$ the growth rate is given as

$$\sigma = -\alpha_i + \mathrm{Real}\Big\{ \frac{1}{\xi} \frac{\partial \xi}{\partial x^1} \Big\}$$

where the first term on the right hand side is the contribution from the exponential part of the disturbance and the second part due to the changes in the amplitude function. The variable $\xi$ is usually $\hat{u}, \hat{v}, \hat{w}, \hat{T}$ or $\bar{\rho}\hat{u} + \hat{\rho}\bar{u}$ taken at some fixed wall normal position or where it reaches its maximum. In addition, the growth rate can be based on the disturbance kinetic energy

$$E = \int_0^{+\infty} \bar{\rho}(|u|^2 + |v|^2 + |w|^2)\, dx^3,$$

and is then written

$$\sigma_{_E} = -\alpha_i + \frac{\partial}{\partial x^1} \ln(\sqrt{E})$$

### 2.4.2. *Step-size restriction*

In the parabolized stability equations presented here no second derivatives of $\hat{\mathbf{q}}$ with respect to $x^1$ exist. The ellipticity has however not entirely been removed. This is known to cause oscillations in the solution as the streamwise step size is decreased. The remaining ellipticity is due to disturbance pressure terms or viscous diffusion terms. Several investigations (see Haj-Hariri 1994; Li & Malik 1994, 1996; Andersson *et al.* 1998) have been performed regarding this problem. Li & Malik showed that the limit for the streamwise step size in order to have stable solution is $1/|\alpha|$. Haj-Hariri proposed a relaxation of the term $\partial\hat{p}/\partial x^1$ in order to allow smaller streamwise steps. Li & Malik showed however that this approach is not sufficient to eliminate the step-size restriction. They showed instead that eliminating $\partial\hat{p}/\partial x^1$ relaxes the step-size restriction. The approach which best removes the ellipticity while still producing an accurate

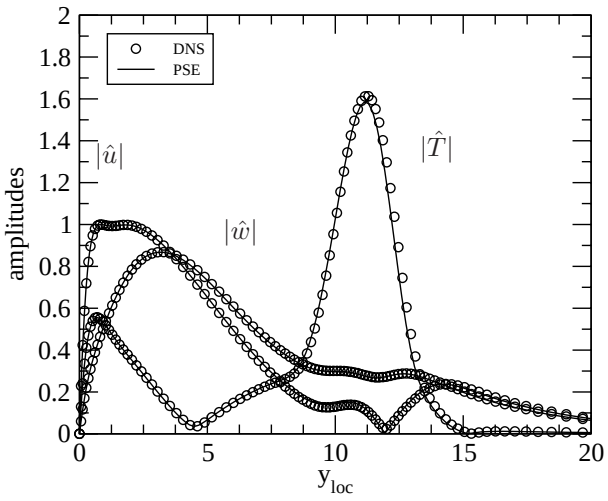


FIGURE 2.1. Comparison of amplitude functions for a second mode instability with $F = 122 \times 10^{-4}$ at $Re = 1900$ between DNS by Jiang *et al.* (2003) and the NOLOT/PSE code for the flow past a flat plate at $M_\infty$=4.5, $T_\infty$=61.11 K, Pr = 0.7, Sutherland's law for viscosity, Stokes hypothesis for the second viscosity.

result is the technique introduced by Andersson *et al.* (1998), where some of the originally neglected higher order terms, $O(Re^{-2})$, are reintroduced in the stability equations. This method is used in the second paper where more details can be found regarding the modifications of the parabolized stability equations.

### 2.4.3. *Comparison with DNS*

Since the development of the Parabolized Stability Equations, several verifications have been made in which the PSE has been compared with the results of Direct Numerical Simulations (DNS), see for instance the investigations by Pruett & Chang (1993); Hanifi *et al.* (1994) and Jiang *et al.* (2003). An example is given here for the case of a flat plate boundary layer with a free stream Mach number $M_\infty$=4.5 and temperature $T_\infty$=61.11 K. The disturbance analyzed is a second mode[3] with reduced frequency $F = 122 \times 10^{-6}$. Here, $F = 2\pi f^* \nu_e^* / U_e^{*2}$ where $f^*, \nu^*$ and $U^*$ are the dimensional frequency, kinematic viscosity and streamwise velocity, respectively. In Figure 2.1, a comparison can be seen between the amplitude functions $\hat{u}, \hat{w}$ and $\hat{T}$ obtained with the NOLOT/PSE code[4] used for the calculations in this thesis and the DNS data provided by Jiang *et al.* (2003). The data has been normalized with the maximum value of $|\hat{u}|$. As can be seen from the figure the agreement is very good.

[3]The second mode is defined in chapter 4.
[4]NOLOT was developed by the authors given in Hanifi *et al.* (1994) and Hein *et al.* (1994)

CHAPTER 3

# Transition prediction

Even though linear theory cannot describe the non-linear phenomena prior and after transition, it has been widely used for transition prediction. Using the linear stability equations previously described, we can calculate the ratio between the amplitudes $A_2$ and $A_1$ which are given at two streamwise positions $X_1$ and $X_2$ as

$$\frac{A_2}{A_1} = \exp\left(\int_{X_1}^{X_2} \sigma dx^1\right).$$

A problem then arises if we say that transition occurs when 'the most dangerous disturbance' reaches a certain threshold amplitude, as the values of $A_1$ and $A_2$ remain unknown. Some empirical methods exist however, where the linear amplification of a disturbance is correlated with the experimentally measured onset of transition. The one which has been mostly used is the $e^N$-method (see van Ingen 1956; Smith & Gamberoni 1956) and a brief review is given here. For an excellent overview of this method see Arnal (1993). As an example we consider the two-dimensional disturbances superimposed on the Blasius boundary layer. If we perform a stability analysis for each streamwise position and for a large number of frequencies $f_1, f_2, \cdots, f_n$ we can draw a neutral curve in the $f - Re$ plane which defines the intersection between the regions where these disturbances are damped and amplified. If the upstream position of the neutral curve (branch one) of a frequency $f_1$ is denoted $X_0$ with its 'initial' amplitude $A_0$, then we can calculate any downstream amplitude $A$ related to the initial one as

$$\frac{A}{A_0} = \exp\left(\int_{X_1}^{X} \sigma dx^1\right) \qquad \text{or} \qquad \ln\left(\frac{A}{A_0}\right) = \int_{X_1}^{X} \sigma dx^1.$$

The frequencies $f_i$ are amplified in different streamwise regions, and the corresponding maximum amplification and streamwise position will therefore vary with frequency. If we take the envelope of the amplification curves over all frequencies as

$$N = \max_f \left[\ln\left(\frac{A}{A_0}\right)\right], \tag{3.1}$$

then at each $x^1$, $N$ represents the maximum amplification factor of these disturbances. Expression (3.1), which is commonly denoted the $N$-factor, cannot however determine the position of transition without additional information.

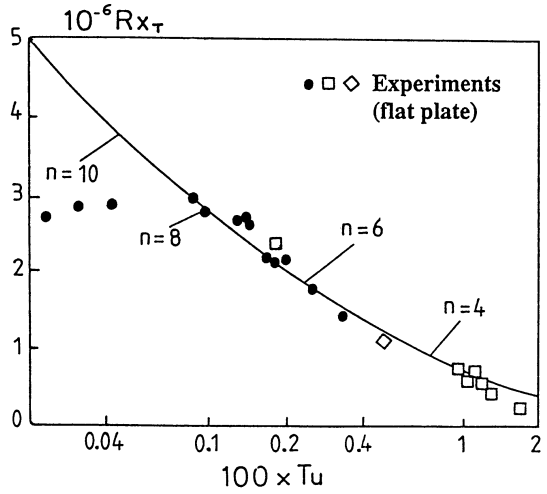


FIGURE 3.1. Comparison between $e^N$-method using expression (3.2) (line), and wind tunnel data (symbols) for a flat plate incompressible boundary layer flow. *(Arnal 1993).*

It was early found in experiments by Smith & Gamberoni (1956) and van Ingen (1956) that the $N$-factor at the transition position was nearly constant ($N_{tr} \approx 7 - 9$). This is unfortunately not universal and does only apply under certain conditions. The disturbances inside the boundary layer can be triggered by acoustic waves, surface roughness, and free stream turbulence. The mechanisms which explain how disturbance enter the boundary layer are commonly called receptivity. Since the route to transition is preceded by receptivity and transition itself involves non-linear mechanisms, their absence in this approach is a shortcoming. Mack (1977) proposed the following expression for the transition $N$-factor to account for dependence of $N_{tr}$ on the free stream turbulence level $Tu$

$$N_{tr} = -8.43 - 2.4 \ln Tu, \tag{3.2}$$

This relation was derived to fit numerical results to low speed zero pressure gradient wind tunnel data. Results of a comparison between expression (3.2) and wind tunnel data can be seen in Figure (3.1). For values of $Tu$ between 0.1% and 1% transition is probably due to exponential instability waves. For higher values of $Tu$, and especially for $Tu > 3\%$ transition occurs at $N = 0$ indicating that transition is not caused by exponential instabilities. In several experiments, (see e. g. Westin *et al.* 1994; Matsubara & Alfredsson 2001), performed at moderate to high free stream turbulence levels, streamwise elongated structures have been observed with streamwise scales much larger than the spanwise scales. A model for transition prediction which correlates well with experimental data from e. g. Matsubara & Alfredsson (2001) for $Tu > 1\%$ was derived by Levin & Henningson (2003). They calculated both exponential

and spatial transient (non-modal) growth of disturbances. For sufficiently large disturbance amplitudes, the latter can lead to the so called bypass transition, which is not associated with exponential instabilities (see e. g. Brandt 2003).

An important issue in applying the $e^N$-method to more complex geometries, where the flow is three dimensional, is the choice of the integration path. For results presented in this thesis we follow the suggestions by Mack (1988). There, applying the condition that the wave number vector is irrotational together with the assumption of a wing with infinite span implies that $\beta$ (spanwise wavenumber) is constant. The $N$-factor is then computed maximizing over $\omega$ and $\beta$. This is here denoted envelope of envelopes (EoE). Due to the shortcomings and limitations of the $e^N$-method mentioned before, better transition prediction models are needed. However, in this thesis the $N$-factor curves should be seen as capturing the trends of variation of the amplification rather than exact prediction of the transition position.

CHAPTER 4

# Disturbance control

The linear stability analysis presented in chapter 2 can be used to calculate the growth of a disturbance superimposed on the mean flow for a given geometry and flow condition. The growth rate can then be used as outlined in chapter 3 for the purpose of transition prediction. In many applications it is also of interest to know how to affect the disturbance growth in order to control the position of laminar-turbulent transition and thus the laminar portion of a given geometry.

The linear stability of compressible boundary layers is different from that of incompressible boundary layers in many ways. The incompressible Blasius boundary layer is stable to inviscid disturbances, as opposed to the compressible boundary layer on an adiabatic flat plate which has a so called *generalized inflection point* and is therefore unstable to inviscid disturbances. The generalized inflection point $y_s$ is defined as the wall normal position where $D(\rho D(U)) = 0$, $(D = \partial/\partial x^3)$. As the Mach number is increased the generalized inflection point moves away from the wall and hence the inviscid instability increases. The viscous instability becomes less significant when $M > 3$, so the maximum amplification rate occurs at infinite Reynolds number and viscosity has a stabilizing instead of destabilizing effect. In incompressible flows there is at most one unstable wave number (frequency) at each $Re$, whereas multiple unstable modes exist whenever there is region of supersonic flow relative to the disturbance phase velocity. The first unstable mode (first mode) is similar to the ones in incompressible flows. The additional modes, which do not have a counter part in incompressible flows, were discovered by Mack (1984) who called them higher modes. The most unstable first-mode waves in supersonic boundary layers are three dimensional, whereas the two-dimensional modes are the most unstable in incompressible boundary layer flows. The most unstable higher mode (second mode) is two-dimensional.

A brief review is made in this chapter on different active and passive methods to act on, or control disturbances in order to affect their amplification. The expression active control implies that energy is added to the flow in order to control, for example suction and blowing at the wall. A passive control on the other hand is made without additional energy added, and an example is changing the curvature of the wall. The review is restricted to methods which will be used later on in the thesis for the purpose of optimal laminar flow

control using blowing/suction, wall temperature distributions, and shape optimization. Other methods which can be used to affect the disturbance growth are e. g. surface roughness, transpiration cooling, nose bluntness and MHD (magneto-hydro-dynamic) flow control.

## 4.1. Suction/blowing

When steady suction is applied, a second inflection point $y_{s1}$ appear close to the wall. This additional inflection point does not destabilize the inviscid disturbances. Masad *et al.* (1991) showed that the suction level needed to remove the generalized inflection point increases with increasing Mach number. They further found that suction is more effective in stabilizing the viscous instabilities and therefore more effective at low Mach numbers. Al-Maaitah *et al.* (1991) showed that suction is more effective in stabilizing second-mode waves at low Mach numbers. They also found that the most unstable second mode remains two-dimensional when suction is applied. In Masad *et al.* (1991) and Al-Maaitah *et al.* (1991) it was found that the variation of the maximum growth rate with suction level is almost linear for both first and second-mode disturbances. Studies have also been performed using discrete suction strips in order to approach a more 'realistic' case where it is assumed that only certain parts of a geometry are available for the implementation of control devices. Masad & Nayfeh (1992) presented results using suction strips for control of disturbances in subsonic boundary layers. They found that suction strips should be placed just downstream of the first neutral point for an efficient control of the most dangerous frequency[1]. However, no such conclusion can be made if all frequencies are considered which is the case in a real experiment. For further reading regarding disturbance control by means of steady suction see the extensive review on numerical and experimental investigations by Joslin (1998).

A different approach to control compared to modifying the mean flow, is to aim the control efforts at the instability wave itself. This is usually called wave cancellation or wave superposition. An advantage of this method is the small amount of control that is needed, of order $O(\epsilon^2)$, in order to obtain considerable reduction of a disturbance with amplitude of order $O(\epsilon)$. The concept of wave superposition has been used in a number of experimental investigations. Milling (1981) used an oscillating wire in water to both introduce and cancel waves. Other investigations concerns elements of heating (Liepmann *et al.* 1982), vibrating ribbons (Thomas 1983), acoustic waves introduced by loudspeakers (Gedney 1983), and suction/blowing (Kozlov & Levchenko 1985). A draw back of this method is that exact information about the amplitude and phase of the disturbance is needed.

[1]The frequency which first reach an $N$-factor which corresponds to laminar-turbulent transition is sometimes denoted 'the most dangerous frequency'.

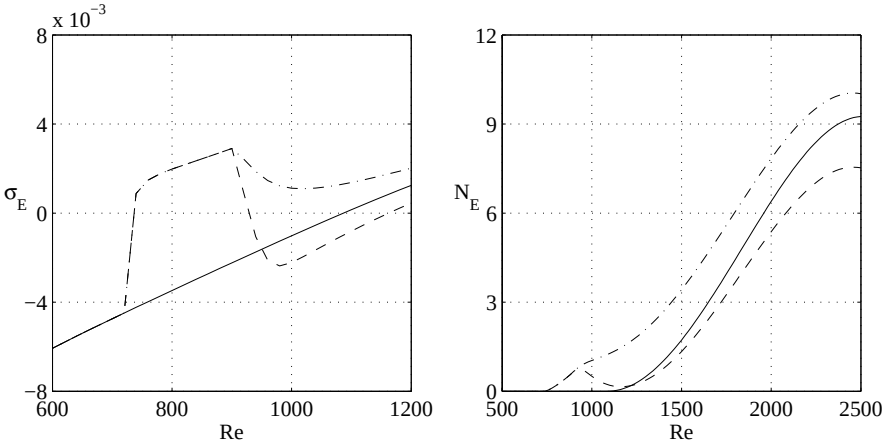


FIGURE 4.1. Disturbance control on a flat plate boundary layer using a heating strip with a temperature of 1.5 times the adiabatic temperature when no control is applied, located at $720 \leq Re \leq 900$. Left: Streamwise variation of the local growth rate of a 2D disturbance with $F = 15 \times 10^{-6}$, for the cases of zero control (solid), compared to the cases when the heating strip is used and the plate downstream of the heating strip is assumed insulated (dash-dot), and heat transfer occurs (dash), $M = 0.8$, $T_\infty = 300$ K, $\Pr = 0.72$. Right: corresponding $N$-factors.

## 4.2. Wall cooling

It was early recognized that uniformly distributed cooling has a damping effect on viscous instabilities of boundary-layer flows at various Mach number, see experiments by e. g. Diaconis *et al.* (1957) and Jack *et al.* (1957). Liepmann & Fila (1947) showed that at low subsonic speeds the transition location on a flat plate moves upstream as it is heated. The destabilizing effect of wall-heating on boundary-layer disturbances is due to the increase of the viscosity of air near the wall, which creates inflectional velocity profiles there. Cooling the wall on the other hand, decrease the viscosity near the wall which results in a thicker velocity profile and thus a more stable flow. Lees & Lin (1946) and Mack (1984) used inviscid and viscous stability theory, respectively, and found that subsonic air boundary layers can be completely stabilized by uniformly distributed wall-cooling. Mack (1984) also showed that uniformly distributed cooling has a destabilizing effect on the higher modes. The results by Mack (1984) have also been confirmed in experiments for supersonic flows by Lysenko & Maslov (1984). In the work by Masad *et al.* (1992) similar results were found using the spatial stability equations for compressible flows. Cooling has an effect on the compressible boundary layer similar to the one found

in boundary layers subject to suction. As cooling is applied an additional inflection point appear close to the surface which is not destabilizing the inviscid disturbances. Masad *et al.* (1992) showed that the cooling level needed to remove the general inflection point increases as the Mach number is increased. They further showed that cooling is always stabilizing the first-mode waves and destabilizing the second-mode waves. Several investigations have also been performed with localized heat-transfer strips. It was found by Masad & Nayfeh (1992) that a properly placed heating strip, close to the first neutral position, has a stabilizing effect on first-mode disturbances. They further showed that a cooling strip at the same location has a destabilizing effect on the first-modes. This effect appear as the flow leaves the cooling strip it encounters a relatively hotter surface downstream, which is destabilizing. The opposite occurs in the case of heating strips. Similar results were found in the numerical investigation by Lo *et al.* (1995) and experiments by Maestrello & Nagabushana (1989). Our investigations showed that this stabilizing effect is found only when the wall-temperature downstream of the strip is set to the adiabatic temperature in the uncontrolled case, $T_{ad_0}$. If the wall is insulated also downstream of the heating strip, the wall-temperature will be larger than $T_{ad_0}$. That is due to the fact that extra heat has been added to the flow as it passes the heating strip. This higher wall-temperature will increase the instability of the flow. This is presented in figure 4.1 and the details regarding these calculations are found in paper 4.

## 4.3. Wall-shaping

Shaping the wall results in two different effects which affect the disturbance instability. The first one is the creation of a pressure gradient and the second one is the effect of surface curvature.

### 4.3.1. *Pressure gradient*

Modification of the pressure gradient can be made by changing either the geometry itself or surrounding conditions. The latter is usually made in wind tunnels by placing a curved geometry above a flat plate. It was early found in experiments for incompressible flows by Schubauer & Skramstad (1948) that a favorable pressure gradient has a stabilizing effect on the boundary layer while the opposite was found for adverse pressure gradients. Malik (1989) investigated the effect of the pressure gradient on second-mode waves at $M = 4.5$. He found that favorable pressure gradients stabilizes the second-mode waves and the band of unstable disturbances moves to higher frequencies. A more thorough investigation was performed by Zurigat *et al.* (1990) in which the pressure gradient was generated assuming a power-law edge Mach-number distribution ($M_e = cx^n$). They analyzed the effects on both the first and second-mode waves at different Mach numbers. They showed that a favorable pressure gradient has a stabilizing effect on both first and second-mode waves. For lower Mach numbers ($M = 2$) oblique first-modes are more efficiently damped than

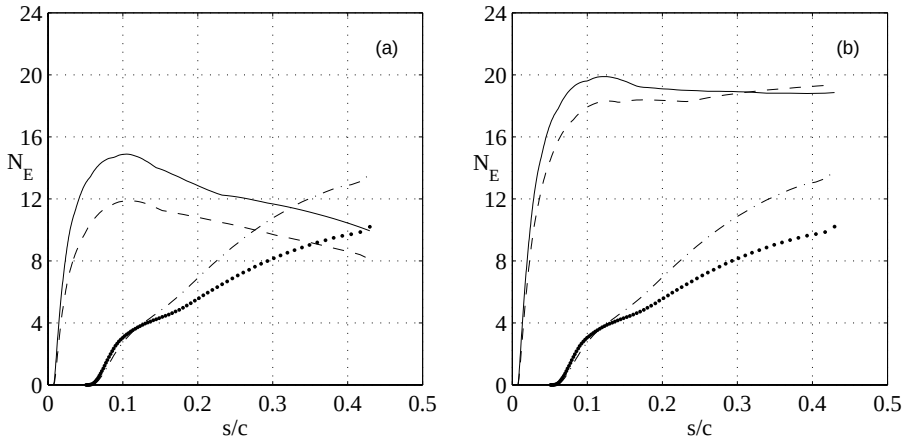


FIGURE 4.2. Effect of including curvature terms in the PSE on the disturbance growth. Envelope of envelopes of $N$-factor curves for cross-flow (CF) and Tollmien-Schlichting (TS) waves. (a) with curvature included; (b) without curvature in the PSE. Traveling CF (Solid), stationary CF (dashed), 2D TS (dotted) and 3D TS (dash-dotted). Mean flow over infinite swept wing with leading edge sweep angle $\psi_{le} = 30.2^o$, Mach number $M_\infty = 0.8$ and temperature $T_\infty = 230$ K.

two-dimensional ones. For higher Mach-numbers ($M = 4 - 8$) it was shown for 2D second-mode waves that the damping effect of a favorable pressure gradient decreases with increasing Mach number. For both disturbance types it was shown that the maximum growth rate varies almost linearly with $n$.

### 4.3.2. *Curvature*

The effects of the curvature on the disturbance growth can roughly be divided into two categories, i. e. those by *concave* surfaces and those by *convex* surfaces. The interest here lies mainly in the case of convex surfaces as such geometries have been analyzed in this thesis. It should however be mentioned that stability analysis of boundary layer flows over concave surfaces has been the topic of many investigations as it concerns the problem of so called Görtler vortices, i. e. stationary counter-rotating vortices arising from centrifugal effects (see e. g. Hall 1983; Spall & Malik 1989). The case of convex surfaces was studied by Masad & Malik (1994) for three-dimensional incompressible flows over an infinite swept cylinder. They found that curvature is stabilizing both stationary and traveling disturbances. Including nonparallel terms, on the other hand, is known to be destabilizing and will therefore have an opposite effect on the disturbance growth compared to curvature. Masad & Malik (1994) found however that the changes in disturbance growth in an analysis accounting for both these effects will be controlled by the convex curvature part.

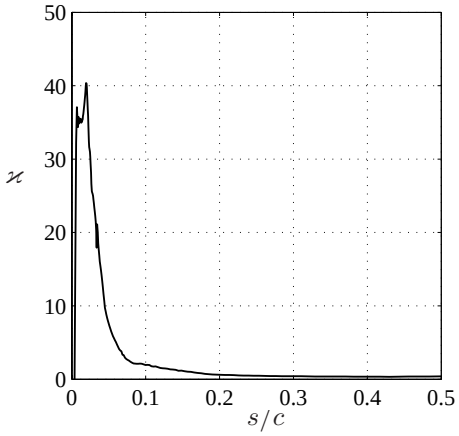


FIGURE 4.3. Curvature, $\varkappa$, of the wing analyzed in Figure 4.2 which is used to calculate the curvature radius $1/\varkappa$.

In the parabolized stability equations used in this thesis, (2.18), the scale factors $h_i$ and corresponding derivatives $m_{ij}$ are all functions of the curvature $\varkappa$. An example on the effect of including curvature in (2.18) or not, is given here. The latter is obtained by setting $h_1 = h_3 = 1$, and corresponding derivatives to zero. The case is the mean flow on the upper surface of an infinite swept wing (see Pralits & Hanifi 2003). Here the envelope of envelopes (EoE) of the $N$-factors for a large number of convectively unstable disturbances have been computed both with and without curvature terms in the linear stability equations. The results are given in Figure 4.2 where the horizontal axis shows the arc-length of the surface divided by the chord length.

The mean flow pressure gradient is strong and negative upstream of $s/c \approx 0.04$ and weak and positive downstream of this position. Due to the inflection point in the velocity profile perpendicular to the inviscid streamline in the region of a favorable pressure gradient, cross-flow (CF) waves are amplified. Further downstream, in the zero or weakly adverse pressure gradient region, Tollmien-Schlichting type of waves are amplified. The curvature $\varkappa$ of the wing can be seen in Figure 4.3. Close to the leading edge the curvature is large and then decreases rapidly downstream until approximately $s/c = 0.05$. Downstream of this position the curvature is an order of magnitude smaller compared to the leading edge. As the region of large curvature coalesce with the region of favorable pressure gradient it is clear that the disturbance growth of CF waves, here given by the $N$-factors, will be mostly affected by the presence of the curvature terms in the linear stability equations.

CHAPTER 5

# Optimal design for disturbance control

The knowledge obtained from the analysis regarding disturbance control, which was previously described, can be used in design of different active and passive devices in order to affect the laminar portion of a geometry such as an aircraft wing. Using suction and blowing, or the wall temperature for control purposes can be considered as active devices. The term design here refers to how the mass flux or temperature should be distributed along the surface. The knowledge regarding the effect of the pressure distribution and curvature on disturbance growth can also be related to the design of the geometry itself. For a rigid body this is made once and can be regarded as a passive control device. A straight forward design approach is, for a given number of design variables, to perform a parameter study in order to find the "best" design. If we take the example of design of a mass flux distribution, this means in practice to test different control domains, mass flux amplitudes, distributions and further more, for each case compute the effect on the disturbance growth. This can be an extremely time-consuming approach if the number of degrees of freedom is large. The word "best" is not objective and its meaning depends on the specific case. For mass flux design it might be to decrease disturbance growth using the least amount of suction power, while for wing design the best could be to decrease disturbance growth while maintaining operational properties such as given lift, and pitch-moment coefficients, and volume. The best solution from a parameter analysis however does not rule out the possibility that an even better solution might exist.

A different design approach is to define an optimization problem with an *objective function* which includes the costs of the design that one wants to minimize using certain *control* or *design variables*. Conditions which should be satisfied while minimizing the objective function are introduced as *constraints*. The advantage of the latter approach is that a number of different optimization techniques such as e. g. gradient-based and generic algorithms exist which depending on the problem can be used to efficiently compute an optimal solution. Gradient-based algorithms are especially efficient when the number of objective functions is small compared to the number of degrees of freedom.

## 5.1. Background

The work related to design of active and passive control devices for disturbance control and transition delay dates back several centuries, and a review

is therefore not made here. Instead an attempt is made to cover representative investigations where optimization techniques have been used for the purpose of disturbance control.

### 5.1.1. *Natural laminar flow*

Design of a geometry such that the laminar portion is increased or maximized is commonly denoted Natural Laminar Flow (NLF) design. In terms of practical implementations, NLF is probably the simplest approach. Once a feasible geometry is found no additional devices such as e. g. suction systems, sensors or actuators need to be mounted. One approach to NLF design is, in a first step, to generate a pressure distribution (target) that delays transition, then, in a second step, design a wing that results in a pressure distribution as close as possible to the target. In addition constraints on e. g. lift, pitch, volume, minimum thickness et cetera must be handled. Green & Whitesides (1996) took an iterative approach which uses a target pressure-N-factor relationship to compute the desired pressure distribution, and an inverse method to find the geometry which satisfies the computed pressure distribution. The $N$-factor method has also been used in multidisciplinary optimization problems of whole aircraft configurations where aerodynamics is considered as one discipline. In Lee *et al.* (1998), it was used to predict the onset of transition in order to determine where to turn on a chosen turbulence model in the Reynolds-Averaged-Navier-Stokes equations, enabling calculation of the friction drag. In Manning & Kroo (1999), a surface panel method was coupled with an approximative boundary layer calculation, and stability analysis. Note however, that none of these investigations explicitly calculates the sensitivity of a quantity obtained from the stability analysis such as the $N$-factor or disturbance kinetic energy, with respect to variations of the geometry. In paper 5, the sensitivity of the disturbance kinetic energy with respect to the geometry is used for the purpose of optimal NLF design.

### 5.1.2. *Laminar flow control*

Laminar flow control (LFC) is an active control technique, commonly using steady suction, to maintain the laminar state of the flow beyond the chord Reynolds number at which transition usually occurs. It is one of the few control techniques which has been attempted in flight tests. A combination of NLF and LFC, where the active control is employed on a just a part of the surface is called hybrid laminar flow control, HLFC. For an extensive review of these techniques see Joslin (1998). Most investigations of HLFC concerns suction but also wall-cooling have been used for control purposes. Balakumar & Hall (1999) used an optimization procedure to compute the optimal suction distribution such that the location of a target $N$-factor value was moved downstream. The theory was derived for two-dimensional incompressible flows and the growth of the boundary layer was not taken into account. In Airiau *et al.*

(2003), a similar problem was solved for the purpose of minimizing the disturbance kinetic energy, accounting for the non-parallel effects using the Prandtl equations and the PSE for incompressible two-dimensional flows. The same problem is extended to three-dimensional incompressible flows in paper 2, and compressible flows on infinite swept wings in paper 3. Similar investigations for the purpose of optimizing temperature distributions are, to the best of our knowledge, not found in the literature. In Masad & Nayfeh (1992), a parameter test was performed to find the "best" location for a predefined temperature distribution in order to reduce the $N$-factor of a given disturbance. In Gunzburger *et al.* (1993) an optimal control problem using boundary controls for the incompressible full Navier-Stokes equations was derived. An application to control by heating and cooling was given with the wall heat flux as the control and a target wall temperature as the objective. In paper 4, a problem is formulated for the purpose of minimizing the disturbance kinetic energy by optimizing the wall temperature distribution. In Hill (1997b) an inverse method was mentioned to compute the optimal suction distributions, and cooling/heating distributions, however no details were given there.

### 5.1.3. *Control by blowing and suction*

In a large number of investigations, different optimal control strategies in a temporal frame work have been investigated. A recent thesis by Högberg (2001) on the topic of optimal control of boundary layer transition provides a good overview of this field. The investigations considered here are performed for spatially developing flows. In Högberg & Henningson (2002), an extension to spatially developing incompressible flows was made for previously developed optimal feedback control through periodic blowing and suction at the wall. Even though parallel flow assumptions are needed for their formulation, successful results are shown for control of TS waves in Blasius flow and cross-flow vortices in Falkner-Skan-Cooke flow. Cathalifaud & Luchini (2000) formulated an optimal control problem for laminar incompressible flows over flat-, and concave walls with optimal perturbations. They successfully minimized both the disturbance kinetic energy at a terminal position, and as streamwise integrated quantity, by optimizing distributions of blowing and suction. In Walther *et al.* (2001) an optimal control problem was derived for two-dimensional incompressible flows with the focus on minimizing the disturbance kinetic energy of TS waves. They accounted for the developing boundary layer using the PSE. In both of the latter investigations, adjoint equations were used to obtain sensitivities of the chosen objective function with respect to the control. A global framework for feedback control of spanwise periodic disturbances, for spatially developing flows, was presented by Cathalifaud & Bewley (2002). In paper 1, we compute the sensitivity of the disturbance kinetic energy in a spatially developing boundary layer flow, with respect to periodic forcing at the wall and inside the boundary layer. The formulation is made using the PSE for compressible flows and the sensitivities are computed using the adjoint of the PSE. The sensitivity of the disturbance kinetic energy with respect to the

wall normal velocity component of the perturbation is used in section 5.4.2 to formulate an optimal control problem for cancellation of instability waves.

## 5.2. Gradient evaluation using adjoint equations

In gradient based optimization, there are different ways to compute the gradients of interest. To discuss this we consider the following problem. Let the state vector $\mathbf{q}$ satisfy the state equation

$$\frac{\partial \mathbf{q}}{\partial x} + A\mathbf{q} = 0; \quad \mathbf{q}(X_0, y) = \mathbf{q}_0, \quad \mathbf{q}(x, 0) = 0, \quad \lim_{y\to\infty} \mathbf{q}(x, y) = 0 \tag{5.1}$$

where $A$ is a matrix. Equation (5.1) is parabolic and solved by integration between $x = X_0$ and $x = X_1$. We wish to find the initial value of $\mathbf{q}(X_0, y) = \mathbf{q}_0$ such that the norm of $\mathbf{q}$ at some downstream position $x = X_1$ defined as

$$\|\mathbf{q}_1\|^2 = \langle \mathbf{q}_1, \mathbf{q}_1 \rangle = \int_0^\infty |\mathbf{q}(X_1, y)|^2 \, dy. \tag{5.2}$$

is maximized. This can be written as an optimization problem where the aim is to maximize an objective function

$$\mathcal{J} = \int_0^\infty |\mathbf{q}(X_1, y)|^2 \, dy, \tag{5.3}$$

where the initial condition $\mathbf{q}_0$ is the control. The gradient of the objective function $\mathcal{J}$ with respect to the control $\mathbf{q}_0$ can be defined through the directional derivative as

$$\delta\mathcal{J} = \langle \nabla\mathcal{J}(\mathbf{q}_0), \delta\mathbf{q}_0 \rangle = \lim_{s\to 0} \frac{\mathcal{J}(\mathbf{q}_0 + s\delta\mathbf{q}_0) - \mathcal{J}(\mathbf{q}_0)}{s} \tag{5.4}$$

A straight forward approach to compute the gradient of interest, $\nabla\mathcal{J}(\mathbf{q}_0)$, is to perturb each degree of freedom of the control and for each perturbation, solve the state equations (5.1) and evaluate the objective function. A finite difference approximation of the gradient can then be made from these results. For a first order finite difference approximation, this is written

$$\nabla\mathcal{J}(\mathbf{q}_0)_i \approx \frac{\mathcal{J}(\mathbf{q}_0 + \epsilon_{\mathbf{q}_0}\mathbf{e}_i) - \mathcal{J}(\mathbf{q}_0)}{\epsilon_{\mathbf{q}_0}} \tag{5.5}$$

where the vector $\mathbf{e}_i$ has component $i$ equal to one and all other components zero, and $\epsilon_{\mathbf{q}_0}$ is a small real-valued parameter. If we denote the number of degrees of freedom $M$, then for a first order approximation of the gradient, the state equations have to be solved $M$ times, for a second order approximation $2M$ times et cetera. If $M$ is large then this procedure can be very time consuming. Another approach which has been shown successful in different optimization problems in fluid dynamics is to use adjoint equations. An example will be given below. For a compact notation of the adjoint equations, we will use the *formal adjoint* $L^*$ for the differential operator $L$ defined by the relation

$$\langle \mathbf{u}, L\mathbf{v} \rangle = \langle L^*\mathbf{u}, \mathbf{v} \rangle + \text{ boundary terms}, \tag{5.6}$$

where the inner product $\langle \cdot, \cdot \rangle$ is defined as

$$\langle \mathbf{u}, \mathbf{v} \rangle = \int_{X_0}^{X_1} \int_0^\infty \mathbf{u}^{\mathrm{T}} \mathbf{v} \, dx \, dy \tag{5.7}$$

for $\mathbb{R}^n$-valued vectors $\mathbf{u}$ and $\mathbf{v}$. Here, the superscript $^*$ stands for the adjoint quantities and $^{\mathrm{T}}$ for the transpose. The derivation of the adjoint equations is made in the following steps: the first variation of equations (5.3) and (5.1) gives

$$\delta \mathcal{J}(\mathbf{q}_0) = 2 \int_0^\infty \mathbf{q}(X_1, y)^{\mathrm{T}} \delta \mathbf{q}(X_1, y) \, dy, \tag{5.8}$$

$$\frac{\partial \delta \mathbf{q}}{\partial x} + A \delta \mathbf{q} = 0, \quad \delta \mathbf{q}(X_0, y) = \delta \mathbf{q}_0, \quad \delta \mathbf{q}(x, 0) = 0, \quad \lim_{y \to \infty} \delta \mathbf{q}(x, y) = 0 \tag{5.9}$$

Then (5.9) is multiplied with the co-state or adjoint variable $\mathbf{r}$ and used in the inner product given by (5.7). The right hand side of (5.6) is derived by removing the derivatives from $\delta \mathbf{q}$ using partial integration

$$\langle \mathbf{r}, \frac{\partial \delta \mathbf{q}}{\partial x} + A \delta \mathbf{q} \rangle = \langle -\frac{\partial \mathbf{r}}{\partial x} + A^{\mathrm{T}} \mathbf{r}, \delta \mathbf{q} \rangle + \Big[ \int_0^\infty \mathbf{r}^{\mathrm{T}} \, \delta \mathbf{q} \, dy \Big]_{X_0}^{X_1}. \tag{5.10}$$

We now require $\mathbf{r}$ to satisfy the adjoint equation with the initial and boundary conditions

$$-\frac{\partial \mathbf{r}}{\partial x} + A^{\mathrm{T}} \mathbf{r} = 0, \quad \mathbf{r}(X_1, y) = 2\mathbf{q}(X_1, y), \quad \mathbf{r}(x, 0) = 0, \quad \lim_{y \to \infty} \mathbf{r}(x, y) = 0. \tag{5.11}$$

Equation (5.11) is integrated from $x = X_1$ to $x = X_0$ and the initial condition for $\mathbf{r}$ at $x = X_1$ is chosen such that the remaining boundary terms can be written

$$\int_0^\infty \mathbf{r}(X_0, y)^{\mathrm{T}} \, \delta \mathbf{q}(X_0, y) \, dy. = 2 \int_0^\infty \mathbf{q}(X_1, y)^{\mathrm{T}} \, \delta \mathbf{q}(X_1, y) \, dy = \delta \mathcal{J}(\mathbf{q}_0) \tag{5.12}$$

Since the left hand side of (5.12) is equal to $\delta \mathcal{J}$, the gradient of $\mathcal{J}$ with respect to $\mathbf{q}_0$ is identified as

$$\nabla \mathcal{J}(\mathbf{q}_0) = \mathbf{r}(X_0, y) \tag{5.13}$$

Compared to the finite-difference approach, the gradient (5.13) is now evaluated by solving the state equation (5.1) and the corresponding adjoint equation (5.11) once, independent of the size of $M$. The right hand side of (5.6) can be derived using either a continuous or discrete approach. A continuous approach means that the adjoint equations are derived from the continuous state equation and then discretized. In the discrete approach, the adjoint equations are derived directly from the discretized state equation. The gradient which is later identified from the adjoint equations, should in the latter case have an accuracy close to machine precision. The accuracy of the gradient derived using the continuous approach increases as the resolution of the computational domain is increased. This is well explained in Högberg & Berggren (2000). The continuous approach has been used through out the thesis except for the work in paper 5 where the adjoint of the inviscid flow equations are derived using

the discrete approach. The accuracy of the numerically calculated gradients is discussed in papers 1, 2 and 5.

## 5.3. Outline of the current approach

In this section the optimal design problems considered in this thesis are outlined. Gradient-based optimization is used in all cases and the gradients of interest are evaluated from the solution of the adjoint equations. The aim is to use different control or design variables in order to achieve a decrease in disturbance growth and therefore an increase in the laminar portion, thus a decrease in friction drag.

### 5.3.1. *Objective function*

The objective function is given as the sum of the different costs of the state which we want to minimize in order to achieve some desired goal. The costs, or cost functions, can be given different weights depending on their respective importance for the goal. In the analysis given here, the cost of friction drag is not given as a measure of the shear stress. It is instead based on the idea that an increase in the laminar portion of the body will result in a decrease of the friction drag. This can also be seen as moving the position of laminar-turbulent transition further downstream. The cost function is therefore a measure which can be related to the transition position. One choice is to measure the kinetic energy of a certain disturbance at a downstream position, say $X_f$. This can be written as

$$E_f = \frac{1}{2}\int_{Z_0}^{Z_1}\int_0^{+\infty} \tilde{\mathbf{q}}^{\mathrm{H}} M \tilde{\mathbf{q}}\; h_1 dx^2 dx^3 \Big|_{x^1=X_f}, \tag{5.14}$$

where $\tilde{\mathbf{q}} = (\tilde{\rho}, \tilde{u}, \tilde{v}, \tilde{w}, \tilde{T})^{\mathrm{T}}$ and $M = \mathrm{diag}(0,1,1,1,0)$ which means that the disturbance kinetic energy is calculated from the disturbance velocity components. If the position $X_f$ is chosen as the upper branch of the neutral curve, then the measure can be related to the maximum value of the $N$-factor as

$$N_{max} = \ln\sqrt{\frac{E_f}{E_0}}, \tag{5.15}$$

where $E_0$ is the disturbance kinetic energy at the first neutral point. If in addition, the value of the $N$-factor of the measured disturbance is the one which first reaches the transition $N$-factor, then the position can be related to the onset of laminar-turbulent transition. It is however not clear, a priori, that such a measure will damp the chosen disturbance or other ones in the whole unstable region, especially if different types of disturbances are present. For Blasius flow, it has been shown that a cost function based on a single TS wave is sufficient to successfully damp the growth of other TS waves (see Pralits *et al.* 2002; Airiau *et al.* 2003). On a swept wing however, it is common that both TS and cross-flow waves are present and moreover can be amplified in different streamwise regions. An alternative is therefore to measure the

kinetic energy as the streamwise integral over a defined domain. Using such an approach several different disturbances, with respective maximum growth rate at different positions, can be accounted for in one calculation. Here, the size of $K$ disturbances superimposed on the mean flow at an upstream position $X_0$, is measured by their total kinetic energy as

$$E_\Omega = \sum_{k=1}^{K} \frac{1}{2} \int_{X_{ms}}^{X_{me}} \int_{Z_0}^{Z_1} \int_{0}^{+\infty} \tilde{\mathbf{q}}_k^{\mathrm{H}} M \tilde{\mathbf{q}}_k h_1 dx^1 dx^2 dx^3. \tag{5.16}$$

We now define the objective function as the sum of all the cost functions based on the disturbance kinetic energy as

$$\mathcal{J}_{\tilde{\mathbf{q}}} = \xi E_\Omega + (1 - \xi) E_f, \tag{5.17}$$

where the parameter $\xi$ can be chosen between zero and one, depending on the quantity we want to minimize. An alternative approach to decrease the disturbance growth and thus increase the laminar portion of the wing was investigated in Airiau *et al.* (2003) to optimize the mean flow suction distribution in a given domain. They minimized the streamwise integral of the shape factor, which for 2D disturbances in a 2D boundary layer should result in a suppression of disturbance amplification. Minimizing the shape factor is a more heuristic approach based on the knowledge that in such flows the two-dimensional disturbances are stabilized by any thinning of the boundary layer. Their results showed that an optimal suction distribution based on minimizing the shape factor does have a damping effect on the disturbance growth. A negative aspect of not explicitly minimizing a measure of the disturbances is that one cannot know if the optimized control will have a damping effect on the disturbances. This has to be calculated after wards. A cost function based on the streamwise integral of the shape factor is here written as

$$\mathcal{J}_{\mathbf{Q}} = \int_{X_{ms}}^{X_{me}} H_{12} h_1 dx^1 = \int_{X_{ms}}^{X_{me}} \frac{\delta_1}{\delta_2} h_1 dx^1, \tag{5.18}$$

where both the displacement $\delta_1$, and momentum-thickness $\delta_2$ are based on the velocity component which is in the direction of the outer streamline. In paper 3 we present results which show that optimal suction distributions obtained by minimizing expression (5.18) does not have a damping effect, but instead amplifies disturbances in the case of swept wing flows.

### 5.3.2. *Optimal design cases*

With the objective functions defined, different optimal design cases can be outlined. We consider the flow over a body decomposed into three different parts: a steady inviscid part provides a pressure distribution $P$ for a given geometry $\mathbf{x}$, a steady mean flow $\mathbf{Q}$ is the solution for a given pressure distribution and geometry, and the solution $\tilde{\mathbf{q}}$ emerging from the stability analysis calculated for a given mean flow and geometry. From the latter, the objective function based on the disturbance kinetic energy can be evaluated. If the objective function

| Design variables | Euler | BLE | PSE | Obj. fcns. | Gradients |
|---|---|---|---|---|---|
| $\tilde{w}_\mathrm{w}$ | $P_0 \rightarrow$ | $\mathbf{Q}_0 \rightarrow$ | $\tilde{\mathbf{q}} \rightarrow$ | $\mathcal{J}_{\tilde{\mathbf{q}}}$ | $\nabla J_{\tilde{\mathbf{q}}}(\tilde{w}_\mathrm{w})$ |
| $\dot{m}_\mathrm{w}, T_\mathrm{w}$ | $P_0 \rightarrow$ | $\mathbf{Q} \rightarrow$ | $\tilde{\mathbf{q}} \rightarrow$ | $\mathcal{J}_{\tilde{\mathbf{q}}}$ | $\nabla J_{\tilde{\mathbf{q}}}(\dot{m}_\mathrm{w}),\ \nabla J_{\tilde{\mathbf{q}}}(T_\mathrm{w})$ |
| $\dot{m}_\mathrm{w}, T_\mathrm{w}$ | $P_0 \rightarrow$ | $\mathbf{Q} \rightarrow$ | | $\mathcal{J}_{\mathbf{Q}}$ | $\nabla \mathcal{J}_{\mathbf{Q}}(\dot{m}_\mathrm{w}),\ \nabla \mathcal{J}_{\mathbf{Q}}(T_\mathrm{w})$ |
| $\mathbf{x}$ | $P \rightarrow$ | $\mathbf{Q} \rightarrow$ | $\tilde{\mathbf{q}} \rightarrow$ | $\mathcal{J}_{\tilde{\mathbf{q}}}$ | $\nabla J_{\tilde{\mathbf{q}}}(\mathbf{x})$ |
| $\mathbf{x}$ | $P \rightarrow$ | $\mathbf{Q} \rightarrow$ | | $\mathcal{J}_{\mathbf{Q}}$ | $\nabla \mathcal{J}_{\mathbf{Q}}(\mathbf{x})$ |
| $\mathbf{x}$ | $P \rightarrow$ | | | $\mathcal{J}_P$ | $\nabla \mathcal{J}_P(\mathbf{x})$ |

TABLE 5.1. Table of state equations involved in the possible optimal design cases. The arrows indicates the order in which the equations are solved, and $P$, $\mathbf{Q}$, and $\tilde{\mathbf{q}}$ are the states obtained by solving the Euler, BLE and PSE respectively. The subscript 0 means that the solution is fixed during the optimization procedure.

is based on the shape factor, only the inviscid and mean flow parts are considered. Three different types of control or design variables are used. In the first, we consider unsteady forcing such as periodic blowing/suction at the wall, $\tilde{w}_\mathrm{w}$, for a fixed geometry. In this case, only the stability equations are affected by the control as the inviscid flow and mean flow are both time-independent and non-linear effects are not accounted for. As a second case we consider control of disturbances by modifications of the mean flow on a fixed geometry. This is made using either a mass flux distribution $\dot{m}_\mathrm{w}$ or a wall temperature distribution $T_\mathrm{w}$. Here both the mean flow and disturbances are affected by the control, which means that an objective function can be based on either $\mathbf{Q}$ or $\tilde{\mathbf{q}}$. The last case considers optimal design by changing the geometry and will affect all states, i. e. the inviscid flow, the mean flow, and the disturbances. It is therefore possible to consider objective functions based on either of the three states $P$, $\mathbf{Q}$ or $\tilde{\mathbf{q}}$.

If we denote the objective functions based on the three different states $P$, $\mathbf{Q}$, and $\tilde{\mathbf{q}}$ as $\mathcal{J}_P$, $\mathcal{J}_{\mathbf{Q}}$, and $\mathcal{J}_{\tilde{\mathbf{q}}}$ respectively, a chart of possible optimal design problems can be made. This is shown in table 5.1. The solution of the inviscid flow, mean flow and disturbances are here denoted Euler, BLE and PSE, respectively. Depending on the design case, one or several states will change during the optimization. The states which are not changed (kept fixed) in respective case are given subscript 0. The different gradients required to solve respective optimization problem are given in the column on the right hand side of table 5.1.

## 5.4. Optimal laminar flow control

### 5.4.1. *Sensitivity analysis using periodic forcing*

The concept of wave cancellation was discussed in section 4.1 and examples were given of experimental results using different types of forcing, or actuators such as heating plates, vibrating ribbons, and blowing and suction. Before deciding which actuator to use in order to control the instability waves, it can be of interest to investigate the sensitivity of different types of forcing $\tilde{\zeta}$ on a measure of the disturbance growth of a given disturbance. The latter is here given by the objective function $\mathcal{J}_{\tilde{\mathbf{q}}}$, expression (5.17). A small variation of the forcing $\delta\tilde{\zeta}$ will cause a small variation of the objective function $\delta\mathcal{J}_{\tilde{\mathbf{q}}}$ and the gradient $\nabla\mathcal{J}_{\tilde{\mathbf{q}}}(\tilde{\zeta})$ express the sensitivity of $\mathcal{J}_{\tilde{\mathbf{q}}}$ with respect to $\tilde{\zeta}$. The different forcing considered here are the disturbance velocity components $\tilde{u}_{\mathrm{w}},\ \tilde{v}_{\mathrm{w}},\ \tilde{w}_{\mathrm{w}}$ and temperature $\tilde{T}_w$ at the wall, and a momentum force $\tilde{\mathbf{S}}$ inside the boundary layer as the model of a vibrating ribbons. When a low amplitude periodic forcing such as blowing/suction at the wall is applied, only the linear stability equations need to be considered, as neither the mean flow nor the inviscid flow is affected if non-linear interaction of the disturbances are neglected. The state equations solved here are the parabolized stability equations outlined in section 2.4, which including the above mentioned periodic forcing are written

$$L_P\,\hat{\mathbf{q}} = \hat{\mathbf{S}}, \tag{5.19}$$

$$\int_0^{+\infty} \hat{\mathbf{q}}^{\mathrm{H}} \frac{\partial \hat{\mathbf{q}}}{\partial x^1} dx^3 = 0. \tag{5.20}$$

The forcing given at the wall are introduced as boundary conditions in (5.19). The gradients of the objective function with respect to each forcing are derived using adjoint equations. This is described in detail in paper 1 and the gradients with respect to the wall forcing are

$$\begin{aligned} \nabla\mathcal{J}_{\tilde{\mathbf{q}}}(\tilde{u}_{\mathrm{w}}) &= \frac{\mu D_3(u^*)}{\bar{\Theta} Re}, \qquad \nabla\mathcal{J}_{\tilde{\mathbf{q}}}(\tilde{v}_{\mathrm{w}}) = \frac{\mu D_3(v^*)}{\bar{\Theta} Re}, \\ \nabla\mathcal{J}_{\tilde{\mathbf{q}}}(\tilde{w}_{\mathrm{w}}) &= \frac{\rho\rho^*}{\bar{\Theta}}, \qquad \nabla\mathcal{J}_{\tilde{\mathbf{q}}}(\tilde{T}_{\mathrm{w}}) = -\frac{\kappa D_3(\theta^*)}{\bar{\Theta}\,\mathrm{Pr}\,Re}, \end{aligned}$$

where $\Theta = e^{i\theta}$, and with respect to the momentum forcing

$$\nabla\mathcal{J}_{\tilde{\mathbf{q}}}(\tilde{\mathbf{S}}) = \frac{\mathbf{q}^*}{\bar{\Theta}} \qquad \text{where} \qquad \mathbf{q}^* = (\rho^*, u^*, v^*, w^*, \theta^*)^{\mathrm{T}}.$$

Here, the over bar denotes the complex conjugate and superscript $*$ denote adjoint variables. The latter satisfy the adjoint of the parabolized stability equations (APSE), here given as

$$L_P^*\,\mathbf{q}^* = \mathbf{S}_P^* \tag{5.21}$$

$$\frac{\partial}{\partial x^1}\int_0^{+\infty} \mathbf{q}^{*\mathrm{H}} \frac{\partial L_P}{\partial \alpha}\,\hat{\mathbf{q}}\,h_1h_2h_3\,dx^3 = f^*, \tag{5.22}$$

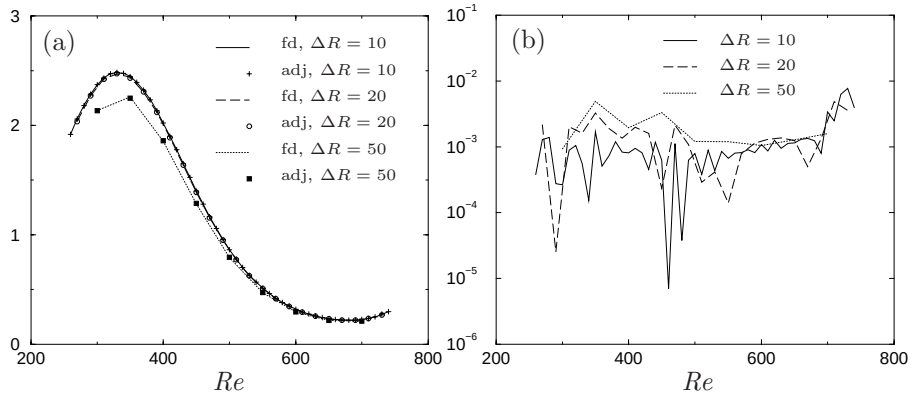


FIGURE 5.1. Comparison between adjoint (adj) and central difference (fd) calculations for different $\Delta R$. Mach number $M = 0.7$, $\beta = 0$. (a) lines denote $||(\partial \mathcal{J}_{\tilde{\mathbf{q}}}/\partial \tilde{w}_r, \partial \mathcal{J}_{\tilde{\mathbf{q}}}/\partial \tilde{w}_i)/\Delta_n||$ and symbols $|\nabla \mathcal{J}_{\tilde{\mathbf{q}}}(\tilde{w}_{\mathrm{w}})_n|$. (b) relative error.

Details regarding equations (5.21)–(5.22) are found in paper 1 for the case of $\mathcal{J}_{\tilde{\mathbf{q}}} = \mathcal{J}_{\tilde{\mathbf{q}}}(\xi = 0)$. The adjoint equations shown here are derived from the continuous state equations. An alternative is to first discretize the state equations and then derive the adjoint equations. It was concluded by Högberg & Berggren (2000) that a continuous formulation is a good enough approximation if control is performed on a problem with a dominating instability. This type of analysis can be made with the PSE and a continuous approach is therefore used here. In order to verify the accuracy of the gradient, we compare the gradients computed using the adjoint equations with those obtained using a finite-difference approximation. In the latter, the gradient of the objective function with respect to each forcing is approximated by a second-order accurate central finite-difference scheme. To compare the gradients given by the adjoint and finite-difference approaches let us consider the example of a wall normal velocity perturbation $\delta\tilde{w}_{\mathrm{w}}$ at $x^3 = 0$. The variation of $\mathcal{J}_{\tilde{\mathbf{q}}}$ with respect to this wall perturbation is :

$$\delta \mathcal{J}_{\tilde{\mathbf{q}}} = \frac{\partial \mathcal{J}_{\tilde{\mathbf{q}}}}{\partial \tilde{w}_r} \delta \tilde{w}_r + \frac{\partial \mathcal{J}_{\tilde{\mathbf{q}}}}{\partial \tilde{w}_i} \delta \tilde{w}_i$$

The subscripts $r$ and $i$ denote the real and imaginary parts of a complex number. In the finite-difference approach, the variation of $\mathcal{J}_{\tilde{\mathbf{q}}}$ is obtained by imposing the inhomogeneous boundary condition $\tilde{w}_{\mathrm{w}} = \pm\varepsilon$ at $x^1 = x^1_n$. Here, $\varepsilon$ is a small number and index $n$ refers to $n$-th streamwise position. Then, the approximative gradients are calculated using a second-order accurate finite-difference scheme. The expression for $\delta \mathcal{J}_{\tilde{\mathbf{q}}}$ in the adjoint approach, for a flat plate geometry, is in discretized form given as

$$\delta \mathcal{J}_{\tilde{\mathbf{q}}} = \int_{Z_0}^{Z_1} \sum_{n=2}^{N-1} \frac{1}{2} (\nabla \mathcal{J}_{\tilde{\mathbf{q}}}(\tilde{w}_{\mathrm{w}})^{\mathrm{H}}_n \delta \tilde{w}_{\mathrm{w}_n} + c.c.) \Delta_n \, dx^2,$$

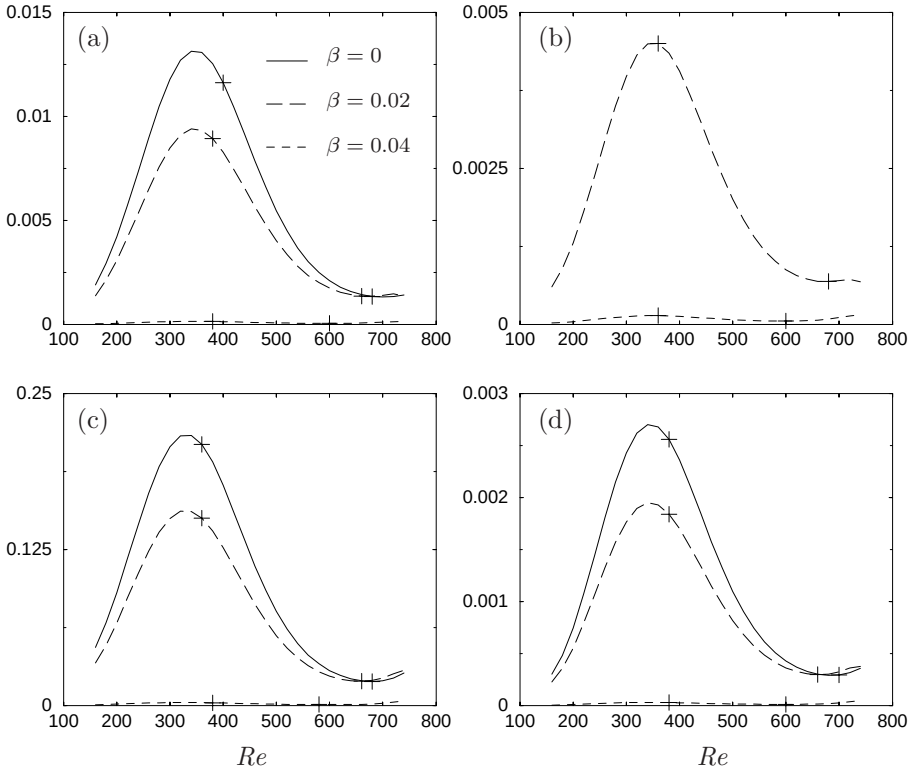


FIGURE 5.2. Modulus of the gradients (sensitivities) due to 2D and 3D wall forcing as a function of the Reynolds number for a flat plate boundary layer at Mach number $M = 0.7$. (a) $|\nabla \mathcal{J}_{\tilde{\mathbf{q}}}(\tilde{u}_{\mathrm{w}})|$, streamwise velocity component; (b) $|\nabla \mathcal{J}_{\tilde{\mathbf{q}}}(\tilde{v}_{\mathrm{w}})|$ spanwise velocity component; (c) $|\nabla \mathcal{J}_{\tilde{\mathbf{q}}}(\tilde{w}_{\mathrm{w}})|$ normal velocity component; (d) $|\nabla \mathcal{J}_{\tilde{\mathbf{q}}}(\tilde{T}_{\mathrm{w}})|$ temperature component. The + marks the first and second neutral point for each case.

where $\Delta_n = (x^1_{n+1} - x^1_{n-1})/2$ and *c.c.* is the complex conjugate. In the following, the quantity $\nabla \mathcal{J}_{\tilde{\mathbf{q}}}(\tilde{w}_{\mathrm{w}})_n$ is compared to those of the finite-difference approach. The case is a flat plate boundary layer with free stream Mach number of 0.7, and the streamwise domain used here is $Re \in [250, 750]$. The modulus $||(\partial \mathcal{J}_{\tilde{\mathbf{q}}}/\partial \tilde{w}_r, \partial \mathcal{J}_{\tilde{\mathbf{q}}}/\partial \tilde{w}_i)/\Delta_n||$, as a function of $x^1_n$, is shown in figure 5.1a and is compared to $|\nabla \mathcal{J}_{\tilde{\mathbf{q}}}(\tilde{w}_{\mathrm{w}})_n|$ for different resolution of the streamwise step $\Delta R$. A good agreement is found between the approaches for a given $\Delta R$, and both values converge as $\Delta R$ is decreased. The relative error given in figure 5.1b is below half a percent for all cases and decreases as $\Delta R$ is decreased. Sensitivity results for a flat plate boundary layer at Mach number $M = 0.7$ subject to two-, and three dimensional wall forcing by $\tilde{u}_{\mathrm{w}}$, $\tilde{v}_{\mathrm{w}}$, $\tilde{w}_{\mathrm{w}}$ and $\tilde{T}_{\mathrm{w}}$ can be seen in figure 5.2. Here the modulus of each component have been plotted as a function of the local Reynolds number. For all cases except the spanwise

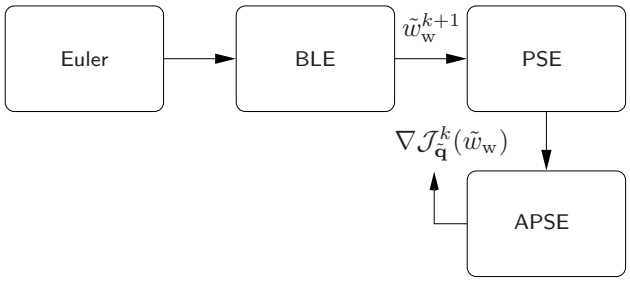


FIGURE 5.3. Flow chart for the case of minimizing the disturbance kinetic energy using the wall normal disturbance velocity at the wall $\tilde{w}_{\mathrm{w}}$.

component, the largest sensitivity is obtained for two-dimensional wall forcing and the maximum value occurs close to the first neutral point of analyzed disturbance. It can also be seen that the magnitude of the wall normal velocity component is about 15 times that of the streamwise component for this case and the ratio is even larger compared to the spanwise velocity component and the temperature. This implies that blowing/suction is the most efficient mean of controlling instability waves. However, as shown in paper 1, the sensitivity decreases with increasing Mach number.

### 5.4.2. *Wave cancellation*

In principle, any periodic forcing considered in section 5.4.1 can be optimized. However, as an example we choose the wall normal velocity component because it has been shown to give the highest sensitivity, and also because it is a good model for periodic blowing/suction. In order to find the optimal solution for a limited cost of the control, and also to bound the control amplitude we define an objective function which balances the cost of the kinetic energy and the control as

$$\tilde{\mathcal{J}}_{\tilde{\mathbf{q}}} = \mathcal{J}_{\tilde{\mathbf{q}}} + l^2 \int_{X_0}^{X_1} |\tilde{w}_{\mathrm{w}}|^2 \, h_1 \, dx^1. \tag{5.23}$$

The term $l^2$ serve as a penalty on the control such that $l^2 = 0$ means unlimited control and vice verse. The gradient of the objective function (5.23) with respect to the control is given as

$$\nabla \tilde{\mathcal{J}}_{\tilde{\mathbf{q}}}(\tilde{w}_{\mathrm{w}}) = \nabla \mathcal{J}_{\tilde{\mathbf{q}}}(\tilde{w}_{\mathrm{w}}) + 2\, l^2 \tilde{w}_{\mathrm{w}} \tag{5.24}$$

As the optimization problem is defined for a given geometry and mean flow, the only state equation which is updated in the optimization procedure is the PSE (5.19)-(5.20). The optimization procedure can now be described considering the chart given in figure 5.3 where $k$ is the iteration number of the optimization loop. An initial disturbance $\tilde{\mathbf{q}}_0$ is superimposed on the mean flow at an initial position $X_0$. The PSE is integrated from $x = X_0$ to $x = X_1$ and the objective function is evaluated. The adjoint equations, APSE are then integrated from $x = X_1$ to $x = X_0$. The gradient is evaluated from the solution of the APSE

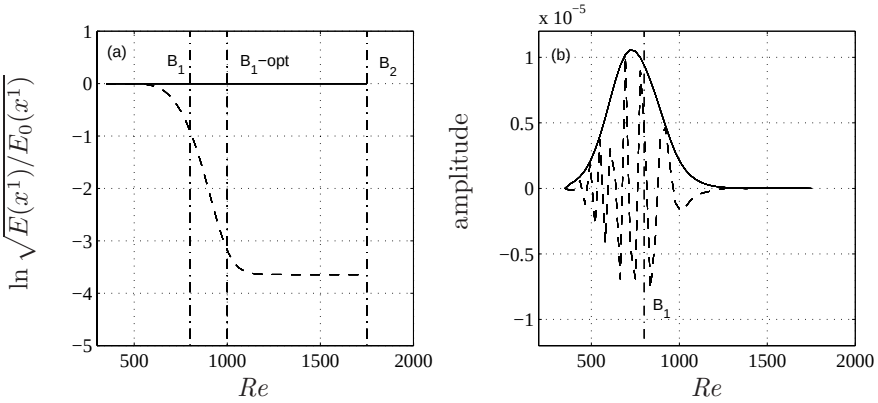


FIGURE 5.4. Control of a two-dimensional wave with $F = 30 \times 10^{-6}$ in a zero pressure gradient flat plate boundary layer where $M_\infty = 0$. (a) energy for zero (solid) and optimal (dashed) control, (b) the optimal suction/blowing distribution given as $|\tilde{w}_\mathrm{w}|$ (solid) and Real($\tilde{w}_\mathrm{w}$) (dashed). $\mathsf{B_i}$ and $\mathsf{B_i}$-opt mark the branch points for zero and optimal control

and the new boundary condition for the PSE is calculated using a chosen optimization algorithm. In the next loop, the PSE is solved with a new $\tilde{w}_\mathrm{w}$ followed by the APSE. The optimization loop is continued until the variation of the objective function is less than a prescribed value. Results of the optimal design problem described above are given in figure 5.4 for the case when $\mathcal{J}_{\tilde{\mathbf{q}}} = \mathcal{J}_{\tilde{\mathbf{q}}}(\xi = 0)$. Here we consider a flat plate boundary layer with free stream Mach number $M_\infty = 0$ and zero pressure gradient. The computational domain in the streamwise direction is $Re = [350, 1750]$. A two-dimensional disturbance with reduced frequency $F = 30 \times 10^{-6}$ is superimposed on the meanflow at $Re = 350$. The control is imposed along the whole plate and the penalty has value of $l = 10^4$. The objective function is evaluated at $Re = 1750$ which is close to the second branch of the neutral curve, i. e. where the disturbance kinetic energy is close to its maximum. In figure 5.4a the reduction in energy has been plotted as the natural logarithm of the ratio between the square root of optimal-, and initial disturbance kinetic energy, $\ln \sqrt{E(x^1)/E_0(x^1)}$. Branch 1 and 2 of the uncontrolled case have been marked with vertical lines as $B_1$ and $B_2$, respectively. The downstream shift of branch one in the case of optimal control is shown with a vertical line marked $B_1 - opt$. In figure 5.4b the optimal distribution of suction and blowing is plotted both as the real part and absolute value. Here it is seen that the control acts most strongly in the vicinity of the first neutral point and then decays rapidly both in the upstream and downstream direction. Results showing that the disturbance kinetic energy measured close to the second branch of the neutral curve is most sensitive to periodic forcing close to the first branch of the neutral curve can be seen in paper 1 for different Mach numbers.

### 5.4.3. *Hybrid laminar flow control*

The motivation for using optimal control theory for the purpose of hybrid laminar flow is that in many industrial applications (see Joslin 1998), the design of e. g. suction systems rely on the experience of the engineers which may not always give the largest delay of laminar-turbulent transition at a given suction power. Design using steady forcing implies that given a fixed geometry, the mean flow will change during the optimization procedure. The analysis here is made using either the wall mass flux $\dot{m}_{\mathrm{w}} = \rho_{\mathrm{w}} W_{\mathrm{w}}$, or the wall temperature $T_{\mathrm{w}}$ as design variables. This particular choice is made as both $\dot{m}_{\mathrm{w}}$ and $T_{\mathrm{w}}$ have been investigated for the purpose of Hybrid Laminar Flow Control. As outlined in table 5.1, several different cases can be considered depending on which combination of objective function and control variable that is used. Gradient based optimization is used in all cases analyzed here and the gradients are evaluated from the solution of adjoint equations. When the objective function is evaluated from the solution of the mean flow, $\mathcal{J}_{\mathbf{Q}}$, then only the BLE is used in the optimization and the gradient of $\mathcal{J}_{\mathbf{Q}}$ with respect to the chosen control variable is evaluated from the adjoint of the boundary layer equations (ABLE). Minimization of $\mathcal{J}_{\tilde{\mathbf{q}}}$ on the other hand, requires the solution of both the BLE and PSE and the respective gradients are evaluated from the ABLE which in turn is forced by the solution of the APSE. A summary on how to compute the gradient for the different cases is given in table 5.2 where $W^*$ and $T^*$ are solutions of the ABLE. Details regarding respective equation are given in papers 3 and 4. Note that for the cases presented in table 5.2 the assumption is made that the streamwise domain of the forcing and the objective function is the same. If this is not the case, changes occur in the boundary conditions of both the BLE and ABLE. This is covered in paper 3 and 4.

#### 5.4.3.1. *Limiting the control*

In many optimization problems it is of interest to bound or limit the control, and in such a way compute the optimal solution using the least effort. Other arguments for bounding the control come from issues regarding validity of the state equations or avoiding ill-posed problems. This can be made using e. g. a regularization parameter such that the objective function express the sum of the original measure, expression (5.17) or (5.18), and a parameter times a defined measure of the control. An example was given in section 5.4.2 for the case of optimizing periodic blowing/suction. As an example here, we consider the case of optimization the wall mass flux to minimize the disturbance kinetic energy. A new objective function can be written

$$\tilde{\mathcal{J}}_{\tilde{\mathbf{q}}} = \mathcal{J}_{\tilde{\mathbf{q}}} + l^2 \int_{X_0}^{X_1} \dot{m}_{\mathrm{w}}^2 \, h_1 \, dx^1. \tag{5.25}$$

The only difference compared to the equations given in table 5.2 appear in the expression of the gradient which is now given as

$$\nabla \tilde{\mathcal{J}}_{\tilde{\mathbf{q}}}(\dot{m}_{\mathrm{w}}) = \nabla \mathcal{J}_{\tilde{\mathbf{q}}}(\dot{m}_{\mathrm{w}}) + 2\, l^2 \dot{m}_{\mathrm{w}}. \tag{5.26}$$

| Des. | Euler | BLE | PSE | Obj. | APSE | ABLE | Gradients |
|---|---|---|---|---|---|---|---|
| $\dot{m}_{\mathrm{w}}$ | $P_0 \rightarrow$ | $\mathbf{Q} \rightarrow$ | $\tilde{\mathbf{q}} \rightarrow$ | $\mathcal{J}_{\tilde{\mathbf{q}}}$ | $\mathbf{q}^* \rightarrow$ | $\mathbf{Q}^* \rightarrow$ | $\nabla\mathcal{J}_{\tilde{\mathbf{q}}}(\dot{m}_{\mathrm{w}}) = W^*_{\mathrm{w}}$ |
| $\dot{m}_{\mathrm{w}}$ | $P_0 \rightarrow$ | $\mathbf{Q} \rightarrow$ | | $\mathcal{J}_{\mathbf{Q}}$ | | $\mathbf{Q}^* \rightarrow$ | $\nabla\mathcal{J}_{\mathbf{Q}}(\dot{m}_{\mathrm{w}}) = W^*_{\mathrm{w}}$ |
| $T_{\mathrm{w}}$ | $P_0 \rightarrow$ | $\mathbf{Q} \rightarrow$ | $\tilde{\mathbf{q}} \rightarrow$ | $\mathcal{J}_{\tilde{\mathbf{q}}}$ | $\mathbf{q}^* \rightarrow$ | $\mathbf{Q}^* \rightarrow$ | $\nabla\mathcal{J}_{\tilde{\mathbf{q}}}(T_{\mathrm{w}}) = \dfrac{\kappa}{Re\,\mathrm{Pr}}\dfrac{\partial T^*_{\mathrm{w}}}{\partial x^3}$ |
| $T_{\mathrm{w}}$ | $P_0 \rightarrow$ | $\mathbf{Q} \rightarrow$ | | $\mathcal{J}_{\mathbf{Q}}$ | | $\mathbf{Q}^* \rightarrow$ | $\nabla\mathcal{J}_{\mathbf{Q}}(T_{\mathrm{w}}) = \dfrac{\kappa}{Re\,\mathrm{Pr}}\dfrac{\partial T^*_{\mathrm{w}}}{\partial x^3}$ |

TABLE 5.2. Table of state and adjoint equations to evaluate respective gradient in the optimal design cases using steady forcing. The arrows indicates the order in which the equations are solved. $P$, $\mathbf{Q}$, and $\tilde{\mathbf{q}}$ are the states obtained by solving the Euler, BLE and PSE respectively, and $\mathbf{Q}^*$ and $\tilde{\mathbf{q}}^*$ are solutions of the ABLE and APSE respectively. The subscript 0 defines that the solution is fixed during the optimization procedure.

If the regularization parameter $l$ is zero then the control is unbounded, and when $l > 0$ then it is bounded. In practice this means that as $l$ is increased, less control effort is allowed, and possibly less decrease in the original state measure is obtained. In some cases it is of interest not only to bound the control but more specifically bound it at a certain value. One example is when the mass flux is optimized for disturbance control purposes. The suction distribution is commonly obtained by a system of pumps and pipes which uses a certain amount of energy. It can therefore be of interest to find an optimal suction distribution which uses a specified amount of energy $E_C$, which for instance can be written as

$$E_C = \int_{X_0}^{X_1} \dot{m}_{\mathrm{w}}^2 \; h_1 \; dx^1. \tag{5.27}$$

In this case the problem is not regularized but instead constrained. As shown in papers 3 and 4, this constraint can be fulfilled using a Lagrange multiplier technique. Details on the derivations are found in the papers and the resulting gradient expression is

$$\nabla\tilde{\mathcal{J}}_{\tilde{\mathbf{q}}}(\dot{m}_{\mathrm{w}}) = \nabla\mathcal{J}_{\tilde{\mathbf{q}}}(\dot{m}_{\mathrm{w}}) + 2\;\chi^*\dot{m}_{\mathrm{w}}, \tag{5.28}$$

The constant regularization parameter $l^2$ in (5.26) has now been replaced by an adjoint variable $\chi^*$. This adjoint variable can be solved as follows: when $\nabla\tilde{\mathcal{J}}(\dot{m}_{\mathrm{w}}) = 0$ then $\dot{m}_{\mathrm{w}} = -W^*_{\mathrm{w}}/(2\chi^2)$ is the corresponding optimal mass flux distribution and usually denoted *optimality condition*, $\dot{m}_{\mathrm{w}}$ is then substituted

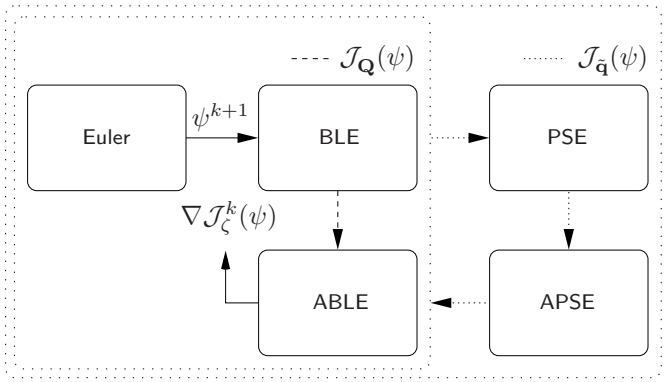


FIGURE 5.5. Optimization procedure using steady forcing. Here, $k$ denotes the iteration number, $\psi$ is the control variable, $\mathcal{J}_{\mathbf{Q}}$ and $\mathcal{J}_{\tilde{\mathbf{q}}}$ are the objective functions evaluated from the solutions of the BLE and PSE respectively.

into (5.27) and an expression for $\chi^*$ is evaluated as

$$\chi^* = \left( \frac{1}{4E_C} \int_{X_0}^{X_1} W_{\mathrm{w}}^{*2} h_1 dx^1 \right)^{\frac{1}{2}}. \tag{5.29}$$

It should be noted that using this approach does not mean that expression (5.27) is satisfied in each iteration of the optimization procedure. The constraint on the control energy is derived assuming that $\nabla \tilde{\mathcal{J}}(\dot{m}_{\mathrm{w}}) = 0$. Therefore, as the optimization problem converge, i. e. $\nabla \tilde{\mathcal{J}}(\dot{m}_{\mathrm{w}})$ goes to zero, also the constraint on the control energy will converge.

5.4.3.2. *Solution procedure*

The optimization procedures for the different optimal design problems considered here can be described using the chart in figure 5.5. There, $k$ denotes the iteration number, $\psi$ is the control variable, $\mathcal{J}_{\mathbf{Q}}$ and $\mathcal{J}_{\tilde{\mathbf{q}}}$ are the objective functions evaluated from the solutions of the BLE and PSE respectively. We start by considering the case of minimizing $\mathcal{J}_{\tilde{\mathbf{q}}}$ for a single disturbance, i. e. $K = 1$ if $\mathcal{J}_{\tilde{\mathbf{q}}}$ includes expression (5.16). This case is presented figure 5.5 as the large dotted rectangle. The optimization is performed for a given geometry and inviscid solution in an iterative procedure. During each iteration step, we perform successive calculations of the BLE and PSE from $X_0$ to $X_1$; and APSE and ABLE from $X_1$ to $X_0$. Then, a new control variable $\psi^{k+1}$ is computed using the gradient evaluated from the solution of the ABLE, in a chosen optimization algorithm. The calculations are repeated until the relative change in the objective function is less than a prescribed value. If the objective function includes expression (5.16) with $K > 1$ then instead of solving both state and adjoint equations $K$ times, we can utilize the fact that the ABLE, here written

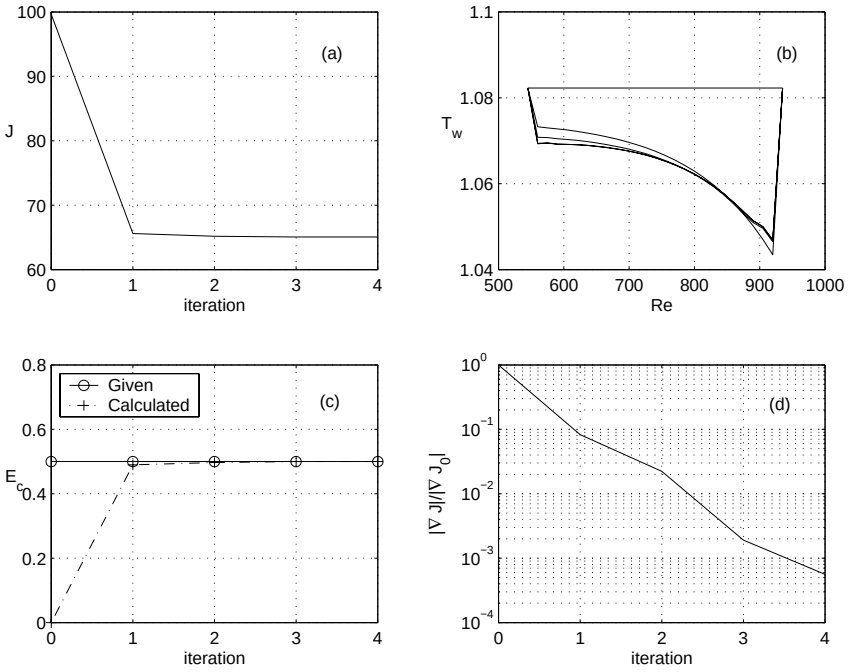


FIGURE 5.6. Convergence history for the case of minimizing the disturbance kinetic energy at a downstream position using the wall temperature. (a) objective function vs. iteration number, (b) wall temperature vs. Reynolds number for all iterations, the arrow shows the direction of increasing iteration number (c) control energy, given and calculated vs. iteration number, (d) gradient norm normalized by its initial value vs. iteration number.

as

$$L_B^* \, \mathbf{Q}^* \quad = \quad S_B^*. \tag{5.30}$$

are linear equations. In this case the gradient is evaluated as follows: the BLE is solved once; the PSE and APSE are solved $K$ times; the right hand side of the ABLE, $S_B^*$, is calculated as

$$S_B^* = \sum_{k=1}^{K} S_{B_k}^*.$$

Finally, the gradient is evaluated from a single calculation of the ABLE. The case of minimizing $\mathcal{J}_{\mathbf{Q}}$ is computationally less expensive. This case is shown in figure 5.5 as the smaller dotted rectangle. During each iteration step, successive calculations are performed of the BLE from $X_0$ to $X_1$; and ABLE from $X_1$ to $X_0$. The gradient evaluation and convergence is then as described above.

5.4.3.3. *Convergence*

An example of the convergence history for an optimal design case is shown in figure 5.6. The wall temperature distribution is optimized such that the disturbance kinetic energy at a downstream position is minimized on a flat plate with zero pressure gradient and a free stream Mach number $M_\infty = 0.7$. A disturbance with reduced frequency $F = 50 \times 10^{-6}$ is superimposed on the meanflow at $Re = 500$ and the objective function, given by expression (5.14), is evaluated at $Re = 935$. The wall temperature distribution $T_\mathrm{w}$ is optimized between $Re = 545$ and $Re = 935$, and the convergence criteria is set as $(\mathcal{J}_{\tilde{\mathbf{q}}}^{k+1} - \mathcal{J}_{\tilde{\mathbf{q}}}^{k})/\mathcal{J}_{\tilde{\mathbf{q}}}^{k} < 10^{-4}$. When control is applied, a deviation of the wall temperature, $\Delta T_\mathrm{w}$, occur with respect to the case of zero control. The constraint used here is the square of $\Delta T_\mathrm{w}$, accounting for both heating and cooling, integrated in the control domain. With the reference temperature taken as the adiabatic wall temperature in the case of zero control $T_{ad_0}$, this is written

$$E_C = \int_{X_{cs}}^{X_{ce}} \Big( T_\mathrm{w} - T_{ad_0}(x^1, 0) \Big)^2 \, dx^1, \tag{5.31}$$

Here, the start and end of the control domain are denoted $X_{cs}$ and $X_{ce}$, respectively, and the value of $E_C$ used in this example is 0.5. The optimization algorithm used here is the L-BFGS-B[1] routine and convergence was reached after 4 iterations. The objective function and the norm of the gradient, normalized by its initial value, both as functions of the iteration number can be seen in figures 5.6a and b, respectively. The objective function has reached a plateau while the gradient norm is still decreasing indicates that the solution is getting close to a local minimum. At the last iteration the relative difference between the given and calculated control energy is $10^{-4}$ (figure 5.6c). If the optimization is continued then finally it would reach a point where the gradient norm would no longer decrease. This might depend on the accuracy of the gradient and/or the search algorithm used. The results from iteration 3 and 4 are not possible to distinguish from each other which can be seen in figure 5.6b, and as efficiency is of importance when a large number of designs are evaluated, the results here are considered converged.

5.4.3.4. *HLFC for an industrial application*

Optimization of the wall temperature or the mass flux distribution without considering how it can implemented and used in a real case might solely be of academic interest or serve as a reference case. This has been addressed in paper 3 for the case of optimizing the mass flux distribution for the purpose of disturbance control on infinite swept wings. The direct application of such an analysis is a tool which could be used in design of HLFC systems. The mass

[1]The algorithm is the limited memory quasi-Newton method developed by Zhu *et al.* (1994). It is based on a limited memory BFGS approximation of the Hessian matrix of the functional $f$, and a gradient projection method is used to account for bounds on the data which makes it suitable for large scale problems where only the gradient of $f$ is available.

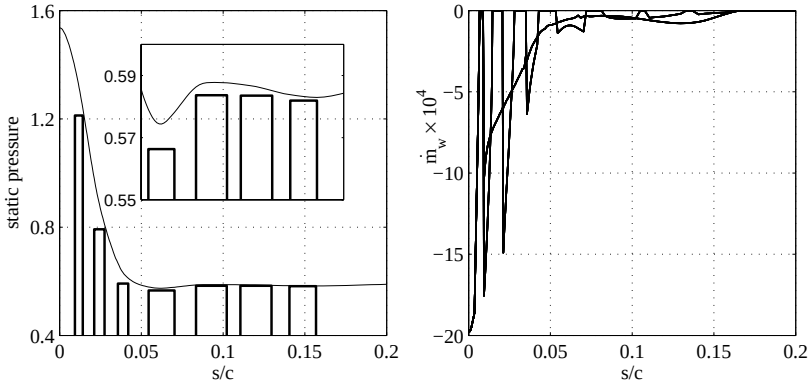


FIGURE 5.7. Optimal suction design for minimization of $E_\Omega$ including a TS and a CF wave. The control energy is $E_C = 0.35$ in all cases. Left: optimal static pressures for the case of 7 pressure chambers, the continuous line shows the pressure distribution on the wing. Right: Corresponding suction distributions (thick lines) compared to an optimal suction distribution in a continuous domain (thin lines).

flux distributions on the porous surface of a wing in these systems is commonly obtained using a number of pressure chambers. The surface velocity can be expressed as a function of the surface porosity, hole geometry and the pressure difference between the pressure distribution on the surface and static pressure in the chambers. The relation used here written on dimensionless form is given as

$$\begin{aligned} \Delta P_j &= P_e - P_{c_j} \\ &= \frac{C_1}{\rho_w}\dot{m}_w^2 + C_2\frac{\mu_w}{\rho_w}\dot{m}_w \quad \forall x^1 \in [X_{cs_j}, X_{ce_j}], \quad j = 1, \cdots, K_p \end{aligned} \tag{5.32}$$

and is taken from Bieler & Preist (1992). It is based on measurements carried out in the framework of the ELFIN (European Laminar Flow INvestigation) program. The internal static pressure, start and end positions of chamber number $j$ is given by $P_{c_j}$, $X_{cs_j}$ and $X_{ce_j}$, respectively, and the coefficients $C_1$ and $C_2$ can be found in paper 3. If we use expression (5.32), then the design variable is no longer $\dot{m}_w$ but instead $P_{c_j}$, and the size and position of the chambers for a given porous surface characterized by $C_1$ and $C_2$. As expression (5.32) is differentiable with respect to $\dot{m}_w$ it is possible to formulate an optimal design problem similar to the previous cases. We use the Lagrange multiplier technique and expression (5.32) is used as an additional constraint. The BLE, PSE, APSE and ABLE are used in the optimization procedure and the gradient of the objective function is now evaluated with respect to $P_{c_j}$. A comparison can now be made between the case of optimizing the mass flux distribution, $\dot{m}_w$, in one continuous domain with the case of optimizing the static pressures

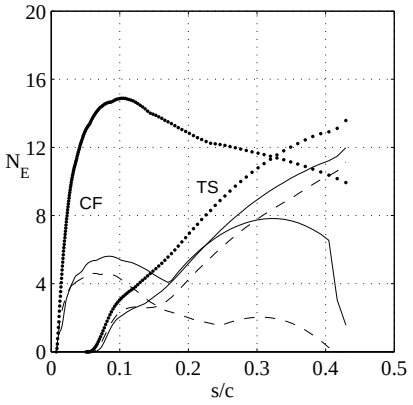


FIGURE 5.8. Envelope of envelopes (EoE) of $N$-factor curves for the cases of zero control (dotted) and the optimal pressure chambers in figure 5.7 (solid). A comparison is made with the EoE of $N_E$-factor curves (dashed) obtained with the continuous suction distribution in figure 5.7.

in a number of discrete pressure chambers, with the aim of minimizing the disturbance kinetic energy. In the latter, $\dot{m}_{\mathrm{w}}$ is indirectly optimized through the relation (5.32). Results taken from paper 3 of such a comparison are presented here for the case of minimizing the disturbance kinetic energy calculated as the sum of a Tollmien-Schlichting (TS) and cross-flow (CF) wave. The mean flow studied is the boundary layer on the upper side of a swept wing designed for commercial aircraft. The continuous mass flux distribution is optimized in the whole available control domain. A configuration of seven pressure chambers are used for the comparison and the start of the first, and end of the last pressure chamber are given by the end points of the available control domain. In both the continuous and pressure chamber cases, the control energy (5.27) is kept constant with a value of 0.35. The left hand side of figure 5.7, shows the optimal static pressures for the case of 7 chambers. The pressure distribution of the wing has been added for comparison in the plot. The largest values of $\Delta P_j$ occur close to the leading edge and then decrease downstream. This is most evident observing the close up made in each plot on the left hand side. The corresponding suction distributions are shown on the right hand side of the same figure. There a comparison is made with the case of optimizing the mass flux in a continuous control domain. Both the continuous suction distribution and the ones obtained from the optimal static pressures are larger in magnitude upstream and then decrease rapidly and become almost constant downstream. The effect on the disturbance growth is given in figure 5.8 by plotting the envelope of envelopes (EoE) of the $N$-factor curves both for TS and CF waves, for the cases of zero and the optimal suction distributions shown in figure 5.7. The results using the continuous suction distribution can be seen as a reference case of what best can be achieved. As further constraints are imposed using

the pressure chambers, it is expected that less damping of the disturbances will be achieved.

## 5.5. Shape optimization for natural laminar flow

The various possible optimal design cases which can be considered in the current frame work, where outlined in table 5.1. In the cases of using the shape of the geometry as design variables, it was shown that the objective function can be based on either the inviscid, mean flow, or stability solution. Note, that in addition, also combinations of the three can be used as an objective function, see paper 5. An objective function based on the solution of the inviscid flow, $\mathcal{J}_P$, is commonly used in the case of shape optimization where the aim is to minimize e. g. the pressure, or wave drag. References to optimization problems regarding inviscid flows can be found in e. g. Jameson (1988). A design problem which accounts for viscous flow effects can be formulated using either $\mathcal{J}_{\mathbf{Q}}$, and/or $\mathcal{J}_{\tilde{\mathbf{q}}}$ as objective function. In particular the latter enables the possibility to account for the physics related to laminar-turbulent transition. In the current approach there are several physical approximations made. A discussion about this is found in paper 5. The goal of the approach taken is to use an iterative gradient-based optimization procedure with the aim of minimizing an objective function based on a measure of the linear disturbance growth by optimizing the shape of the geometry, such as a wing. As a decrease in disturbance growth means a downstream shift of the laminar-turbulent transition location, and thus an increase of the laminar portion of the surface, the approach taken here can be seen as optimal design for natural laminar flow.

### 5.5.1. *Problem formulation and gradients*

We minimize the objective function based on the disturbance kinetic energy $\mathcal{J}_{\tilde{\mathbf{q}}}$, expression (5.17), which depends explicitly on the solution of the stability equations $\tilde{\mathbf{q}}$ and the mesh, here given by the nodal coordinates $\mathbf{X}$. This is here written as

$$\mathcal{J} \equiv \mathcal{J}(\tilde{\mathbf{q}}, \mathbf{X}) \,, \tag{5.33}$$

and is evaluated as follows:

1. The solution of the Euler equations for compressible flows (see paper 5) provides the pressure distribution of a given geometry
2. The viscous mean flow is obtained by solving (2.5)–(2.8) for the given geometry, and the pressure distribution from the Euler solution.
3. The parabolized stability equations (2.18)–(2.19) are solved for the geometry, and mean flow from the boundary layer analysis.
4. The objective function (5.33) is evaluated from the solution of the parabolized stability equations.

If $\mathbf{w}$, $\mathbf{Q}$, and $\tilde{\mathbf{q}}$ are the solutions of the three state equations given above, then $\mathcal{J}$ can be considered to be a functional of $\mathbf{X}$ only and the objective function is then denoted $\mathcal{J}_X(\mathbf{X})$. The nodal coordinates, $\mathbf{X}$, are evaluated from the

displacements, $\mathbf{y}$, of the nodes on the airfoil by a mesh movement algorithm, here denoted $\mathbf{X} \equiv \mathbf{X}(\mathbf{y})$. The displacements are controlled by the parameter $\mathbf{a}$, i. e. $\mathbf{y} \equiv \mathbf{y}(\mathbf{a})$. From these definitions we can now define

$$\mathcal{J}_y(\mathbf{y}) = \mathcal{J}_X(\mathbf{X}(\mathbf{y})), \quad \text{and} \quad \mathcal{J}_a(\mathbf{a}) = \mathcal{J}_y(\mathbf{y}(\mathbf{a})), \tag{5.34}$$

which clearly shows that $\mathcal{J}_a(\mathbf{a})$ is the objective function depending only on the control parameter $\mathbf{a}$. As the gradient of $\mathcal{J}_a(\mathbf{a})$ with respect to $\mathbf{a}$ is used in the optimization procedure, we show in paper 5 that $\nabla\mathcal{J}_a$ can be evaluated from

$$\nabla\mathcal{J}_X \quad \rightarrow \quad \nabla\mathcal{J}_y \quad \rightarrow \quad \nabla\mathcal{J}_a,$$

in the above mentioned order. The gradient of the objective function with respect to the nodal coordinates $\nabla\mathcal{J}_X$ is derived using adjoint equations and is evaluated solving the APSE, ABLE and adjoint of the Euler equations (AEuler) in the mentioned order.

### 5.5.2. *Mesh displacements, parametrization and geometrical constraints*

All displacements are made with respect to a reference mesh, defined by its vector of nodal coordinates $\mathbf{X}^0$. For a vector $\mathbf{y}^k$ of shape displacements the new grid is obtained as

$$\mathbf{X}^k = \mathbf{X}^0 + \mathrm{L}\mathbf{y}^k. \tag{5.35}$$

Given the gradient $\nabla J_X$ of a functional $J_X$ of the nodal coordinates, the gradient of the functional $J_y(\mathbf{X}) \equiv J_X(\mathbf{X}(\mathbf{y}))$ is obtained by the following matrix–vector product

$$\nabla\mathcal{J}_y = \mathrm{L}^T\nabla\mathcal{J}_{\mathbf{X}}. \tag{5.36}$$

Smooth shapes, together with geometric constraints, are obtained taking the vectors of displacements $\mathbf{y}$ that are the solutions of a minimization problem (see Amoignon 2003) of the form

$$\mathbf{y} = \begin{cases} \min\limits_{\mathbf{v}\in\mathbb{R}^n} \dfrac{1}{2}\mathbf{v}^T\mathrm{A}_s\mathbf{v} - \mathbf{v}^T\mathrm{M}_s\mathbf{a}, \\ \mathrm{C}^T\mathbf{y} = \mathbf{b}, \end{cases} \tag{5.37}$$

where $\mathrm{A}_s$ is the stiffness matrix associated with the Laplace operator, $\mathrm{M}_s$ is a mass matrix, C is the matrix whose rows are the gradients of the linear constraints (in $\mathbb{R}^{n\times m}$) and $\mathbf{b}$ is the vector of values imposed to the constraints (in $\mathbb{R}^m$). The solution $\mathbf{y}$ to the above system can be seen as the vector of displacements, which, according to the norm defined by the positive definite matrix $\mathrm{A}_s$, is the closest to the solution of the discretized Laplace equation defined by

$$\mathrm{A}_s\tilde{\mathbf{y}} = \mathrm{M}_s\mathbf{a}, \tag{5.38}$$

and fulfills exactly the constraints

$$\mathrm{C}^T\mathbf{y} = \mathbf{b}. \tag{5.39}$$

Such a parameterization implies that the controls are the vector $\mathbf{a}$, right hand side of equation (5.38), and the vector $\mathbf{b}$, right hand side of the constraints,

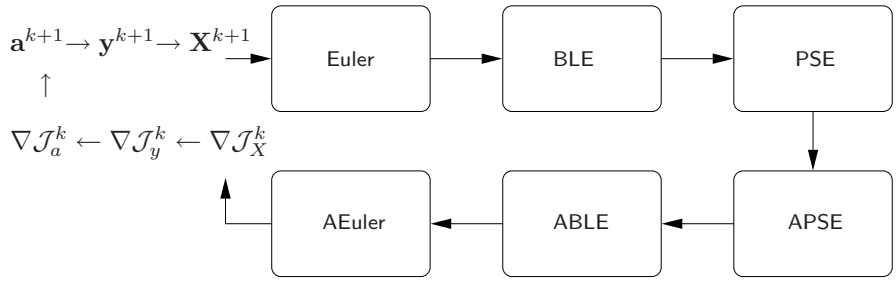


FIGURE 5.9. Flow chart for the case of minimizing the disturbance kinetic energy using the parameter **a** to control the shape of geometry.

relation (5.39). The gradients with respect to **a** and **b**, which are the control variables in our method, can then be obtained by solving an adjoint problem (see Amoignon 2003) of the form

$$\begin{pmatrix} A_s^T & -C \\ -C^T & 0 \end{pmatrix} \begin{pmatrix} \mathbf{y}^* \\ \lambda^* \end{pmatrix} = \begin{pmatrix} \nabla \mathcal{J}_y \\ \mathbf{0} \end{pmatrix}, \tag{5.40}$$

from which it holds that

$$\nabla \mathcal{J}_a = M_s^T \mathbf{y}^* \quad \text{and} \quad \nabla \mathcal{J}_b = -\lambda^* . \tag{5.41}$$

Note that $\nabla \mathcal{J}_y$ in (5.40) is obtained by evaluating expression (5.36). All constraints considered so far are equality constraints, and **b** is therefore a vector of constants. The only control parameter in this case is therefore **a**.

### 5.5.3. *Solution procedure*

A simple chart of the order in which the state and adjoint equations are solved and gradients are evaluated in order to perform optimal NLF is given in figure 5.9. There, $k$ denotes the iteration number and the procedure is as follows:

1. For $k = 1$, we start with an initial Euler mesh $\mathbf{X}^0$
2. The Euler, BLE and PSE are solved in the given order
3. The objective function $\mathcal{J}^k$ is evaluated
4. The adjoint equations, APSE, ABLE and AEuler are solved
5. The gradients $\nabla \mathcal{J}_X^k$, $\nabla \mathcal{J}_y^k$ and $\nabla \mathcal{J}_a^k$ are evaluated in the given order
6. A new control parameter $\mathbf{a}^{k+1}$ is calculated[2] using the gradient $\nabla \mathcal{J}_a^k$
7. If $k > 1$, check convergence: If $|(\mathcal{J}^{k+1} - \mathcal{J}^k)/\mathcal{J}^k| < \epsilon$, else[3] continue
8. A new mesh $\mathbf{X}^{k+1}$ is calculated from the new control parameter $\mathbf{a}^{k+1}$
9. Goto 2.

[2]In the computations shown in paper 5, the L-BFGS-B routine was used, normally requiring several functional and gradient evaluations in order to build up the approximative Hessian matrix.

[3]Several convergence criteria exist in the L-BFGS-B routine, (see Zhu *et al.* 1994)

### 5.5.4. *An optimal design case*

An optimization case in which constraints are not imposed on operational properties such as lift, and pitch-moment coefficients might result in a design which is not useful. Results are shown here for the case of minimizing an objective function including both the disturbance kinetic energy, pressure drag $C_D$, and in addition penalties on the deviations of the lift, and pitch-moment coefficients, $C_L$ and $C_M$, from the initial values. This is written

$$\mathcal{J}_C = \lambda_U \mathcal{J} + \lambda_D C_D + \lambda_L \frac{1}{2}\left(C_L - C_L^0\right)^2 + \lambda_M \frac{1}{2}\left(C_M - C_M^0\right)^2 , \qquad (5.42)$$

where the coefficients $\lambda_U$ and $\lambda_D$ are used to normalize $\mathcal{J}$ and $C_D$ with respective values computed using the initial mesh. The coefficients $\lambda_L$ and $\lambda_M$ are used to penalize the deviations of $C_L$ and $C_M$ from respective values computed on the initial mesh. The initial design is the RAE2822 airfoil and the flow is characterized by a free stream Mach number of $M_\infty = 0.734$ and Reynolds number of $Re_\infty = 6.5 \times 10^6$. The disturbance used to evaluate $\mathcal{J}$ has a physical frequency $f^* = 11$ kHz and wave angle of $\psi_w \approx 40^\circ$ and is integrated from close to the leading edge to half chord. As geometrical constraints we impose that the volume should not deviate from its initial value and that a region around the leading edge is kept fixed.

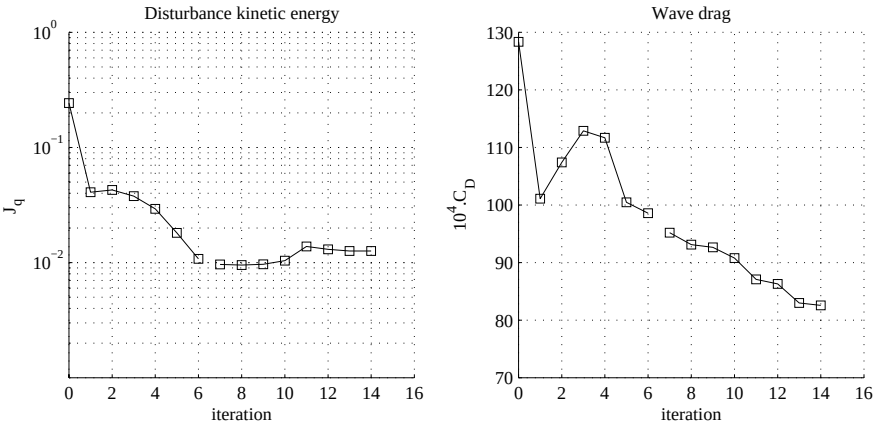


FIGURE 5.10. Left: Disturbance kinetic energy. Right: wave drag. Both as functions of the iteration number.

Results of the convergence history is shown in figures 5.10 and 5.11 for the disturbance kinetic energy, pressure drag, lift, and pitch-moment coefficients as functions of the iteration number. A reduction in the objective function (5.42) is obtained from the first to the last iteration (see paper 5). During a few iterations, however, it can be noted that the pressure drag increase while the deviations of $C_D$ and $C_M$ decrease, figure 5.10. At the final iteration a

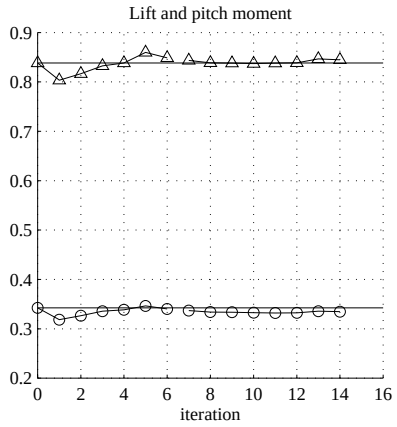


FIGURE 5.11. Lift, (triangle-solid) and pitch-moment (circle-solid) coefficients as functions of the iteration number. The values at initial design are indicated at each step (solid).

reduction has been obtained in both disturbance kinetic energy and pressure drag while $C_D$ and $C_M$ are kept within a few percent, figure 5.11.

A comparison between the pressure coefficients, and geometry for the initial (solid) and last iteration (dash) obtained from the optimization can be seen in figure 5.12. The largest change in the geometry occur in the region on the upper side of the airfoil where $\mathcal{J}$ is evaluated. This can also be seen in the pressure distributions. The relative small change on the lower side is caused in order to satisfy the constant volume constraint. As the upper side of the final design is thinner, and the part around the leading edge is fixed to approximately 4% chord, an increase occur in the curvature of the airfoil around 10% chord. This can be seen in the decrease in the pressure coefficient in that region.

The EoE of the $N$-factor curves for a large number of modes can be seen in figure 5.13 for the initial and final design. In comparison with figure 5.12 we can note that the pressure gradient in the region where the disturbance become unstable has change from an adverse to zero or weakly favorable. This has a damping effect on the disturbance growth in the whole domain where $\mathcal{J}$ is evaluated, which can be seen in figure 5.13. In order to estimate the change in the total drag computations were performed solving the Reynolds Averaged Navier Stokes equations on the initial and final design. The transition location in these computations was estimated using the EoE curves computed using the pressure distributions from the Euler solutions. The computations showed a decrease in pressure drag of about 25%, viscous drag of about 23%, and total drag of about 24%. In the approach taken here there are still improvements to be made. This can for instance be seen looking at the region $x/c \approx 0.4$ to $x/c \approx 0.6$ of the pressure distributions in figure 5.12 of the final design. The

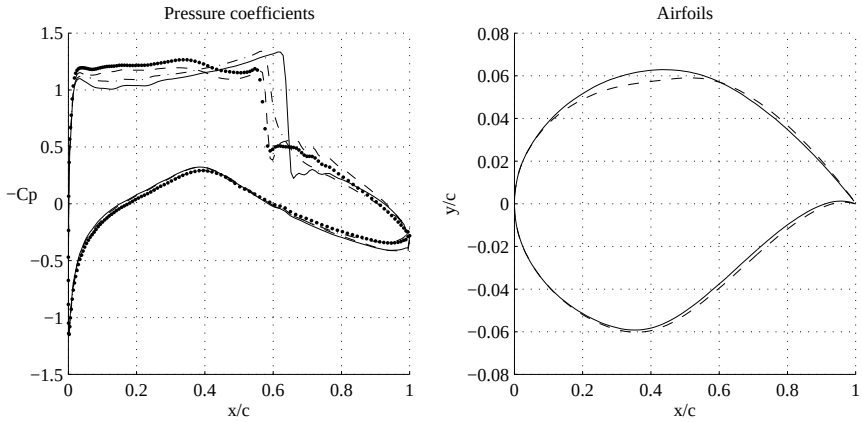


FIGURE 5.12. Left: Pressure coefficients for initial (solid), and final design (dash) obtained from the optimization solving the Euler equations. A comparison is made using the Reynolds Averaged Navier Stokes Equtions to compute the flow of the initial (dash-dot), and final design (dot). Right: initial (solid) and final design (dash).

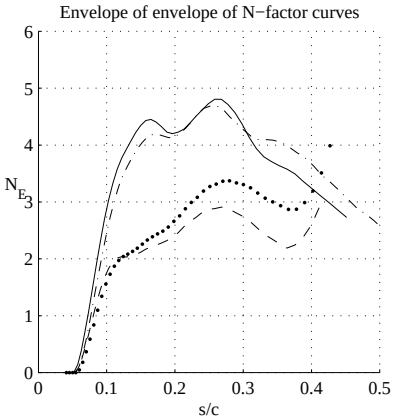


FIGURE 5.13. Envelope of envelopes of $N$-factor curves. Lines correspond to the cases shown in figure 5.12.

pressure gradient in this region is adverse indicating that separation occurs. More results and discussions are found in paper 5.

CHAPTER 6

# Summary & conclusions

The work presented in this thesis concerns the use of gradient-based optimization techniques for the purpose of laminar flow control (LFC), and design of wings for natural laminar flow (NLF). The goal of using this technique is to reduce the viscous drag. Reduction of viscous drag can be seen as an increase of the laminar portion of the wing, thus a delay of laminar-turbulent transition. On wings in low free-stream turbulence environments, the latter is usually caused by break down of small disturbances which grow as they propagate down stream. The fluid flow has been divided into three different parts, namely: an inviscid part providing the pressure distribution for a given geometry, a viscous mean flow which is computed given the pressure distribution and geometry, and finally a linear stability analysis using the PSE providing the growth rate of convectively unstable disturbances superimposed on the viscous mean flow. The growth rate can been used to predict the transition location using the so called $e^N$-method. Here it is assumed that transition will occur at the location where the total amplification of the disturbance, with respect to the first streamwise position where the disturbance starts to grow, attains an empirically determined value, whose logarithm is generally denoted by $N$.

Several optimization problems have been defined for the purpose of LFC and NLF with the aim of minimizing an objective function based on measures of, or related to, the growth of unstable disturbances. Here, different control variables, means of control, have been used and the gradients of the objective function with respect to the control has been derived using adjoint equations. Especially the derivation of the adjoint of the PSE (APSE), and the adjoint of the BLE (ABLE) for compressible flows have been of interest, and now accomplished can be used in several applications. An existing optimization routine has been used in most cases as the topic of this research does not concern development of these routines.

The accuracy of the gradients evaluated from the solution of the adjoint equations have been investigated by comparing them with those computed by a finite-difference approximation. The tests have shown that an increased accuracy can be achieved by increasing the spatial resolution of the discretized equations. As the latter is known to cause numerical stability problems for the PSE, a known method to overcome this problem has been used which also alters the APSE and ABLE. A sensitivity analysis using the gradients of the disturbance kinetic energy at the second neutral point with respect to periodic

forcing show that control is most efficiently made in the vicinity of the first neutral point. It was further shown that the disturbance kinetic energy is most sensitive to control by means of periodic blowing and suction, and in general the efficiency decreases with increasing Mach number.

Results of optimal steady suction distributions have been presented for both incompressible and compressible flows. It has been shown that minimizing an objective function based on the disturbance kinetic energy of a single disturbance results in a suction distribution which has a damping effect on a large number of disturbances of the same type, e. g. (TS) Tollmien-Schlichting-, or (CF) cross-flow waves. On swept wings, a situation might occur when both these types of waves exist simultaneously. For such cases it has been shown that both types must be included in the objective function in order to obtain a suction distribution which has a damping effect on other disturbances of these two types. Results of optimal temperature distributions for disturbance control have been presented for various Mach numbers. It has been shown that the efficiency of the optimal control decreases when the wall temperature downstream of the control domain is maintained at its original adiabatic value, compared to the case when the wall there is insulated. It has also been shown that the efficiency decreases with increasing Mach number.

A problem has been formulated to perform optimal NLF design, in which the aim is to minimize a measure of the disturbance kinetic energy. Results have been presented for cases where both the disturbance kinetic energy, and wave drag have been reduced simultaneously while lift, and pitch-moment coefficients as well as the volume have been maintained at desired values.

One of the goals with work presented here was to show that the derived techniques can be used in realistic applications. This was addressed for the case of optimal suction distributions in which the problem was also formulated using discrete pressure chambers, and computations were made on an infinite swept wing designed for commercial aircraft. Also the problem of optimal NLF design was formulated such that airfoils in realistic flow conditions can be optimized.

# Acknowledgment

I want to thank my advisor Professor Dan Henningson for being so supportive, encouraging and always available to assist in questions regarding the world of fluid mechanics as well as personal matters. It has been a long and interesting journey and I consider myself fortunate for the freedom I have been given to proceed, with my sometimes endless derivations, knowing that there was always support.

I want to thank my assistant advisor Doctor Ardeshir Hanifi for sharing his knowledge as well software which has given me a very good basis from which to start this work. He has spend many hours explaining theoretical matters, supporting me in the European projects and been a really good friend.

I want to thank Doctor Martin Berggren for many useful discussions which have provided more consistency in the mathematical formulations regarding the adjoint equations.

I want to acknowledge Professor Alessandro Bottaro and Doctor Christophe Airiau for the good cooperation which started in 1999, and the hospitality they showed me during my stay in Toulouse in October, 2000.

This work has been funded by the Swedish Foundation for Strategic Research (SSF) through the Integral Vehicle Structures (IVS)-program and partially by the Swedish Defence Research Agency (FOI), and the EU project (ALTTA contract G4RD-CT-2000-00143).

I want to acknowledge the colleagues in the ALTTA project for all the interesting discussions as well as good company.

Many thanks to everyone at the Department of Mechanics for the good company, fika, innebandy and nice atmosphere. In particular I want to mention: Luca Brandt (V), Markus Högberg, Ruben Wetind, Martin Skote, Nulifer Ipek, Astrid Herbst, Ori Levin, Jérôme Hoepffner, Mattias Chevalier, Gustaf Mårtensson, Arnim Brüger, Johan Gullman-Strand, Fredrik Lundell, Björn Lindgren och Jens Fransson.

Thanks Olivier for the good collaboration we had working on SEBAS.

En stor kram till min familj och vännerna i södertälje och ett speciellt tack till FF&SB.

*Karimah, gioia della mia vita, grazie che tu esisti* : $\star$

# Bibliography


Airiau, C. 2000 Non-parallel acoustic receptivity of a Blasius boundary layer using an adjoint approach. *Flow, Turbulence and Combustion* **65**, 347–367.

Airiau, C., Bottaro, A., Walther, S. & Legendre, D. 2003 A methodology for optimal laminar flow control: Application to the damping of Tollmien-Schlichting waves in a boundary layer. *Phys. Fluids* **15**, 1131–1145.

Al-Maaitah, A. A., Nayfeh, A. H. & Masad, J. A. 1991 Effect of suction on the stability of supersonic boundary layers. part I: Second-mode waves. *J. Fluids Engng* **113**, 591–597.

Amoignon, O. 2003 Aerodynamic shape optimization: I. *Tech. Rep.*. Department of Information Technology, Uppsala, Sweden, licenciate thesis to be published, University of Uppsala.

Andersson, P., Henningson, D. S. & Hanifi, A. 1998 On a stabilization procedure for the parabolic stability equations. *J. Engng Maths* **33**, 311–332.

Arnal, D. 1993 Boundary layer transition: Predictions based on linear theory. Special course on 'progress in transition modeling', March-April 1993. AGARD-R-793, 2-1–2-63.

Balakumar, P. & Hall, P. 1999 Optimum suction distribution for transition prediction. *Theor. Comput. Fluid Dyn.* **13**, 1–19.

Bertolotti, F. P. 1998 The influence of rotational and vibrational energy relaxation on boundary-layer stability. *J. Fluid Mech.* **372**, 93–118.

Bertolotti, F. P., Herbert, T. & Spalart, S. 1992 Linear and nonlinear stability of the Blasius boundary layer. *J. Fluid Mech.* **242**, 441–474.

Bieler, H. & Preist, J. 1992 HLFC for commercial aircraft. In *First european forum on laminar flow technology*, pp. 193–199. Hamburg.

Brandt, L. 2003 Numerical studies of bypass transition in the Blasius boundary layer. PhD thesis, Royal Institute of Technology, Stockholm, Sweden.

Cathalifaud, P. & Bewley, T. R. 2002 A numerically tractable global framework for the feedback control of boundary-layer perturbations. ASME, ASME Fluids Engineering Division Summer Meeting, Montreal, Canada.

Cathalifaud, P. & Luchini, P. 2000 Algebraic growth in a boundary layer: optimal control by blowing and suction at the wall. *Eur. J. Mech. B/Fluids* **19** (4), 469–490.

Diaconis, N. S., Jack, J. R. & Wisniewski, R. J. 1957 Boundary-layer transition

at mach 3.12 as affected by cooling and nose blunting. *NACA Tech. Note No. 3928* .

Dobrinsky, A. & Collis, S. S. 2000 Adjoint parabolized stability equations for receptivity prediction. *AIAA Paper* (2000-2651).

Gaster, M. 1974 On the effect of boundary layer growth in flow stability. *J. Fluid Mech.* **66**, 465–480.

Gedney, C. J. 1983 The cancellation of a sound-excited Tollmien-Schlichting wave with plate vibration **26** (5), 1158–1160.

Green, B. E. & Whitesides, J. L. 1996 A method for the constrained design of natural laminar flow airfoils. *AIAA Paper* (96-2502).

Gunzburger, M. D., Hou, L. S. & Svobodny, T. P. 1993 The approximation of boundary control problems for fluid flows with an application to control by heating and cooling. *Comp. Fluids* **22** (2/3), 239–251.

Haj-Hariri, H. 1994 Characteristics analysis of the parabolized stability equations. *Stud. Appl. Math.* **92**, 41–53.

Hall, P. 1983 The linear development of görtler vortices in growing boundary layers. *J. Fluid Mech.* **130**, 41–58.

Hanifi, A., Henningson, D. S., Hein, S. & Bertolotti, F. P.and Simen, M. 1994 Linear non-local instability analysis - the linear NOLOT code. *FFA TN* **1994-54**.

Hein, S., Bertolotti, F. P., Simen, M., Hanifi, A. & Henningson, D. S. 1994 Linear non-local instability analysis - the linear NOLOT code. *DLR-IB* **223-94 A 43**.

Herbert, T. 1997 Parabolized stability equations. *Annu. Rev. Fluid Mech.* **29**, 245–283.

Herbert, T. & Bertolotti, F. P. 1987 Stability analysis of nonparallel boundary layers. *Bull. Am. Phys. Soc.* **32**, 2079.

Hill, D. C. 1997a Receptivity in non-parallel boundary layers. In *ASME Fluids Engineering Division Summer Meeting, FEDSM '97*.

Hill, D. C. 1997b Inverse design for laminar three-dimensional boundary layers. *Bull. Am. Phys. Soc.* **42**, 2120.

Högberg, M. 2001 Optimal control of boundary layer transition. PhD thesis, Royal Institute of Technology, SE-172 90 Stockholm, Sweden.

Högberg, M. & Berggren, M. 2000 Numerical approaches to optimal control of a model equation for shear flow instabilities. *Flow, Turbulence and Combustion* **65**, 299–320.

Högberg, M. & Henningson, D. S. 2002 Linear optimal control applied to instabilities in spatially developing boundary layers. *J. Fluid Mech.* **470**, 151–179.

van Ingen, J. L. 1956 A suggested semiempirical method for the calculation of the boundary layer transition region. *Tech. Rep.* VTH-74. Department of Aeronautical Engineering, University of Delft.

Itoh, N. 1986 The origin and subsequent development in space of Tollmien-Schlichting waves in a boundary layer. *Fluid Dyn. Res.* pp. 119–130.

Jack, J. R., Wisniewski, R. J. & Diaconis, N. S. 1957 Effects of extreme surface cooling on boundary-layer transition. *NACA Tech. Note No. 4094* .

Jameson, A. 1988 Aerodynamic design via control theory. *J. Scientific Computing* **3** (3), 233–260.

Jiang, L., Chang, C.-L., Choudhari, M. & Liu, C. 2003 Cross-validation of DNS and PSE results for instability-wave propagation in compressible boundary layers past curvilinear surfaces. *AIAA Paper* (2003-3555), 33rd AIAA Fluid Dynamics Conference and Exhibit, Orlando, Florida, 23-26 June, 2003.

Joslin, R. 1998 Overview of laminar flow control. *Tech. Rep.* 1998-208705. NASA, Langley Research Center, Hampton, Virginia.

Kozlov, V. V. & Levchenko, V. Y. 1985 Laminar-turbulent transition control by localized disturbances. *AIAA Paper* (85–0568).

Lee, J.-M., Schrage, D. P. & Mavris, D. N. 1998 Development of subsonic transports with laminar flow wings. *AIAA Paper* (98-0406).

Lees, L. & Lin, C. C. 1946 Investigation of the stability of the laminar boundary layer in a compressible fluid. *NACA Tech. Note No. 1115* .

Levin, O. & Henningson, D. S. 2003 Exponential vs algebraic growth and transition prediction in boundary layer flow. *Flow, Turbulence and Combustion* Accepted for publication.

Li, F. & Malik, M. R. 1994 Mathematical nature of parabolized stability equations. In *4th IUTAM Symp. on Laminar-Turbulent Transition, Sendi, Japan* (ed. R. Kobayashi), pp. 205–212. Springer.

Li, F. & Malik, M. R. 1996 On the nature of PSE approximation. *Theor. Comput. Fluid Dyn.* **8**, 253–273.

Liepmann, H. W., Brown, G. L. & Nosenchuck, D. M. 1982 Control of laminar-instability waves using a new technique. *J. Fluid Mech.* **118**, 187–200.

Liepmann, H. W. & Fila, G. H. 1947 Investigations of effects of surface temperature and single roughness elements on boundary-layer transition. *NACA Tech. Report No. 890* .

Lo, C. F., Lafrance, R., Meredith, W. S. & Wiberg, C. G. 1995 Laminar flow control with wall temperature distribution for quiet supersonic wind tunnels. *AIAA Paper* (95-2296).

Lysenko, V. I. & Maslov, A. A. 1984 The effect of cooling on supersonic boundary-layer stability. *J. Fluid Mech.* **147**, 39–52.

Mack, L. M. 1977 Transition prediction and linear stability theory. Paris: AGARD Report No 224, also JPL Publication 77-15, 1977.

Mack, L. M. 1984 Boundary-layer linear stability theory. *AGARD Report No. 709* .

Mack, L. M. 1988 Stability of three-dimensional boundary layers on swept wings at transonic speeds. In *IUTAM Symp. Transsonicum III* (ed. J. Zierep & H. Oertel). Göttingen: Springer.

Maestrello, L. & Nagabushana, K. A. 1989 Relaminarization of turbulent flow on a flat plate by localized surface heating. *AIAA Paper* (89-0985), 2nd Shear Flow Conference, March 13-16, 1989/Tempe, AZ.

Malik, M. R. 1989 Prediction and control of transition in supersonic and hypersonic boundary layers. *AIAA J.* **27**, 1487–1493.

Malik, M. R. & Balakumar, P. 1992 Nonparallel stability of rotating disk flow using PSE. In *Instability, Transition and Turbulence* (ed. M. Hussaini, A. Kumar & C. Streett), pp. 168–180. Springer.

Manning, V. M. & Kroo, I. M. 1999 Multidisciplinary optimization of a natural laminar flow supersonic aircraft. *AIAA Paper* (99-3102).

Masad, J. A. & Malik, M. R. 1994 Effects of body curvature and nonparllelism on the stability of flow over a swept cylinder. *Phys. Fluids* **6**, 2363–2379.

Masad, J. A. & Nayfeh, A. H. 1992 Laminar flow control of subsonic boundary layers by suction and heat-transfer strips. *Phys. Fluids A* **4** (6), 1259–1272.

Masad, J. A., Nayfeh, A. H. & Al-Maaitah, A. A. 1991 Effect of suction on the stability of supersonic boundary layers. part II: First-mode waves. *J. Fluids Engng* **113**, 598–601.

Masad, J. A., Nayfeh, A. H. & Al-Maaitah, A. A. 1992 Effect of heat transfer on the stability of compressible boundary layers. *Comp. Fluids* **21** (1), 43–61.

Matsubara, M. & Alfredsson, P. 2001 Disturbance growth in boundary layers subjected to free-stream turbulence. *J. Fluid Mech.* **430**, 149–168.

Milling, R. W. 1981 Tollmien-Schlichting wave cancellation **24** (5), 979–981.

Pralits, J. O., Airiau, C., Hanifi, A. & Henningson, D. S. 2000 Sensitivity analysis using adjoint parabolized stability equations for compressible flows. *Flow, Turbulence and Combustion* **65** (3), 321–346.

Pralits, J. O. & Hanifi, A. 2003 Optimization of steady suction for disturbance control on infinite swept wings. *Phys. Fluids* **15** (9), 2756–2772.

Pralits, J. O., Hanifi, A. & Henningson, D. S. 2002 Adjoint-based optimization of steady suction for disturbance control in incompressible flows. *J. Fluid Mech.* **467**, 129–161.

Pruett, C. D. & Chang, C.-L. 1993 A comparison of PSE and DNS for high-speed boundary-layer flows. In *Transitional and Turbulent Compressible Flows* (ed. L. Kral & T. Zang), , vol. 151, pp. 57–67. Washington, D.C.: ASME.

Saric, W. S. & Nayfeh, A. H. 1975 Non-parallel stability of boundary layer flows. *Phys. Fluids* **18**, 945–950.

Schubauer, G. B. & Skramstad, H. K. 1948 Laminar-boundary-layer oscillations and transition on a flat plate. *NACA Tech. Note No. 909* .

Simen, M. 1992 Local and non-local stability theory of spatially varying flows. In *Instability, Transition and Turbulence* (ed. M. Hussaini, A. Kumar & C. Streett), pp. 181–201. Springer.

Smith, A. M. O. & Gamberoni, N. 1956 Transition, pressure gradient and stability theory. *Tech. Rep.* ES 26388. Douglas Aircraft Co.

Spall, R. E. & Malik, M. R. 1989 Goertler vortices in supersonic and hypersonic boundary layers. *Phys. Fluids A* **1**, 1822.

Thomas, A. S. W. 1983 The control of boundary-layer transition using a wave-superposition principle. *J. Fluid Mech.* **137**, 233–250.

Walther, S., Airiau, C. & Bottaro, A. 2001 Optimal control of Tollmien-Schlichting waves in a developing boundary layer. *Phys. Fluids* **13**, 2087–2096.

Westin, K., Boiko, A., Klingmann, B., Kozlov, V. & Alfredsson, P. 1994 Experiments in a boundary layer subjected to free stream turbulence. part 1. boundary layer structure and receptivity. *J. Fluid Mech.* **281**, 193–218.

Zhu, C., Byrd, R., Lu, P. & Nocedal, J. 1994 L-BFGS-B: Fortran subroutines for large scale bound constrained optimization. *Tech. Rep.* NAM-11. EECS Department, Northwestern University.

Zurigat, Y. H., Nayfeh, A. H. & Masad, J. A. 1990 Effect of pressure gradient on the stability of compressible boundary layers. *AIAA Paper* (90-1451), 21st Fluid Dynamics, Plasma Dynamics and Lasers Conference, Seattle, WA.